STRUCTURAL INVESTIGATION OF ESSENTIAL ENZYMES IN PATHOGENIC BACTERIA AND EVALUATION OF DRUG CANDIDATES

A Dissertation

by

CORY CALVIN THURMAN

Submitted to the Office of Graduate and Professional Studies of Texas A&M University in partial fulfillment of the requirements for the degree of

DOCTOR OF PHILOSOPHY

Chair of Committee,	James C. Sacchettini
Co-Chair of Committee,	Richard Gomer
Committee Members,	Gary Kunkel
	Thomas Meek
Interdepartmental Program Chair,	David Threadgill

May 2019

Major Subject: Genetics

ABSTRACT

The cell wall is a common component found in nearly all bacteria. Long validated as a drug target for over half of all prescribed antibiotics, it continues to offer new sources for increasing that number ever further. Eschewing the ubiquitous transpeptidase-targeting beta lactams, pathways for the biosynthesis of the rhamnose linker between peptidoglycan and arabinogalactan, and peptidoglycan itself, provide alternatives for developing novel antibiotics to pathogenic bacteria.

The first half of this study will focus on the four-member pathway responsible for the production of dTDP-L-rhamnose and includes a structural analysis of some members found in *Mycobacterium tuberculosis (Mtb)* in conjunction with their respective inhibitors. The specific architecture of each individual inhibitor inside the active site of the enzyme offers insight into the role each atom plays in binding and explains why small variations of the compound influence this relationship. This same variation also affects the ability of the compound to reach its target inside the cell.

The second half of this study will focus on the first step of the pathway for biosynthesis of uridine diphosphate N-acetylmuramic acid pentapeptide, the immediate precursor to peptidoglycan. UDP-N-acetylglucosamine enolpyruvyl transferase (MurA) catalyzes the transfer of the enolpyruvyl moiety of phosphoenolpyruvate to the 3’ hydroxyl group of UDP-N-acetylglucosamine, yielding enolpyruvyl-UDP-N-acetylglucosamine and phosphate. This enzyme is highly conserved among bacteria and found as a single copy in gram negative bacteria.

DEDICATION

I would like to dedicate this work to my mother and father for their support and patience on my journey to completing my PhD.

ACKNOWLEDGEMENTS

I would like to thank my committee chair Dr. Sacchettini for the opportunity to do this research, as well as my committee members Dr. Gomer, Dr. Kunkel, and Dr. Meek for their time and guidance.

I would like to acknowledge Liam Guthrie and Andres Silva for their work on the mouse and compound solubility/bioavailability experiments.

CONTRIBUTORS AND FUNDING SOURCES

This work was supervised by a dissertation committee consisting of Professor James Sacchettini (advisor), Professor Richard Gomer (co-advisor) and Professors Gary Kunkel and Thomas Meek.

This work was made possible in part by the National Institutes of Health under Grant Number P01AI095208. Its contents are solely the responsibility of the authors and do not necessarily represent the official views of the Texas A&M University.

TABLE OF CONTENTS

Page

ABSTRACT.....ii

DEDICATION.....iv

ACKNOWLEDGEMENTS.....v

CONTRIBUTORS AND FUNDING SOURCES.....vi

TABLE OF CONTENTS.....vii

LIST OF FIGURES.....viii

LIST OF TABLES.....ix

CHAPTER I INTRODUCTION AND LITERATURE REVIEW.....1

CHAPTER II STRUCTURAL AND FUNCTIONAL INSIGHTS INTO INHIBITION OF THE RHAMNOSE BIOSYNTHESIS PATHWAY AND THE TRIAZINOINDOL-BENZIMIDAZOLONES IN MYCOBACTERIUM TUBERCULOSIS
Overview.....48
Introduction.....49
Materials and Methods.....51
Results.....64
Discussion.....72

CHAPTER III STRUCTURAL AND FUNCTIONAL INSIGHTS INTO INHIBITION OF UDP-N-ACETYLGLUCOSAMINE ENOLPYRUVYL TRANSFERASE IN PSEUDOMONAS AERUGINOSA
Overview.....83
Introduction.....84
Materials and Methods.....88
Results.....93
Discussion.....100

CHAPTER IV CONCLUSION AND FUTURE DIRECTIONS.....104

REFERENCES.....108

APPENDIX.....134

LIST OF FIGURES

FIGURE Page

1. Structure of L-rhamnose.....1
2. Diagram of *M. tuberculosis* cell wall.....13
3. Representation of the rhamnose pathway.....18
4. Mimicry between penicillin and D-ala-D-ala.....33
5. Representation of the MurA pathway.....37
6. Triazinoindol-benzimidazolone analogs.....67
7. RmlD inhibitor compounds.....68
8. Triazinoindol-benzimidazolone scaffold and IC50's..69
9. 5 RmlC inhibitor structures overlayed.....72
10. 7093044 structure.....74
11. 7093044 structure showing effects of R2 sub.....76
12. Docking structure of RmlC-6892686.....79
13. RmlC-6892686 structure.....80
14. RmlC-7093044 electrostatic map.....81
15. Cytotoxicity data of inhibitors.....82
16. Ligplot diagram of 7093044 interactions.....83
17. PAO1 whole cell assay.....94
18. MurA-product structure.....95
19. Sequence alignment of MurA from PDB.....96
20. Overlay of pathogenic MurA structures.....98
21. PEP hole in MurA-product structure.....103

LIST OF TABLES

TABLE Page

1. Plasma protein binding results.....70

CHAPTER I

INTRODUCTION AND LITERATURE OVERVIEW

The ability of pathogenic bacteria to elude antibiotics presents an ever present and increasing threat to the worldwide human health. Various forms of evolutionary adaptations have rendered some antibiotics virtually ineffective. Research continues onward to improve validated classes of antibiotics, in conjunction with creating new ones. The differential nature of the bacteria cell wall relative to eukaryotic cells has made it a vast and extensively probed target and will continue to do so for the foreseeable future.

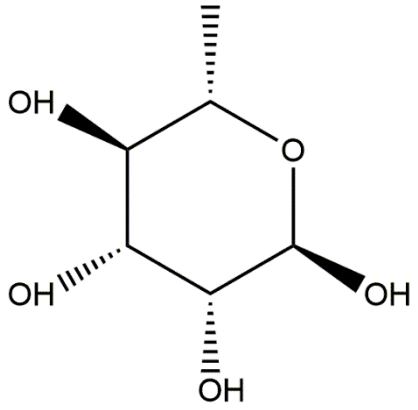

L-Rhamnose

Figure 1: Structure of L-Rhamnose

Rhamnose is found in nature in both the L- and D-forms. While no usage or dietary requirement has been discovered in humans, rhamnose can be found in bacteria, archaea, plants, fungi, and even viruses[3-8]. The biosynthetic process is similar across organisms, beginning with glucose. The enzymes differ in their exact mechanism, including bifunctional enzymes, but the basic four steps, transferase, dehydratase, epimerase, and reductase, are maintained. The final form of rhamnose, dTDP-L-rhamnose, UDP-L-rhamnose, GDP-D-rhamnose, GMP-D-rhamnose, depends on the specific usage, which depends on the organism. *Pseudomonas aeruginosa* utilizes both the L- and D-forms, for rhamnolipids and lipopolysaccharides, respectively[7]. The archaeon *Thermoplasma acidophilum* metabolizes L-rhamnose as its sole carbon source[9]. A small number of viruses, such as *Acanthocystis turfacea* chlorella virus 1 and *Acanthamoeba polyphaga* mimivirus, utilize UDP-L-rhamnose for posttranslational modification of their capsid proteins[6]. *Arabidopsis thaliana* requires UDP-L-rhamnose for the biosynthesis of the pectic polysaccharide rhamnogalacturonan-I, needed for proper orientation of microtubules[10].

In most bacteria, rhamnose is not required for survival. A lack of rhamnose may affect overall fitness or the ability to sustain a pathogenic infection but may not constitute an absolute requirement[8]. The position or levels of rhamnose determine whether the *rml* genes are essential. For instance, *Pseudomonas aeruginosa* can survive without rhamnose but its ability to infect is severely compromised[11]. However, in some bacteria such as the human pathogen *Streptococcus pyogenes*, roughly half of the cell wall is comprised of a rhamnose-rich polysaccharide[12]. *Mycobacterium tuberculosis*, and all *Mycobacterium* species studied to date, employ dTDP-L-rhamnose to incorporate a rhamnosyl linker into the cell wall, connecting the peptidoglycan layer to the arabinogalactan layer[13]. In both of these cases, rhamnose is absolutely essential for survival. The specific and singular use in *Mycobacterium tuberculosis* has led to the rhamnose pathway being considered a candidate for a novel antibiotic. The first section of this record of study evaluates the biochemical and structural nature of the enzymes of the pathway, in conjunction with evaluations of inhibitors and analogs to determine binding characteristics.

Rhamnose is used for wide variety of purposes in plants, from structural to seed coatings, and even the color of flowers reflected in rhamnosylated anthocyanins found within the petals[4, 10, 14]. The pathway is similar to that found in bacteria, in that a diphosphonucleotide-charged rhamnose (NDP-rhamnose) is produced. However, most plants, such as *Arabidopsis thaliana*, combine the last two steps within a single bifunctional enzyme roughly twice the size of the bacterial homologues comprising RmlC and RmlD[4]. This bifunctional enzyme is expressed as a polypeptide which also includes the RmlB dehydratase activity in the N-terminal region. Sequence alignments offer additional evidence. The N-terminal region of RHM2 strongly aligns with bacterial examples of RmlB[15]. The C-terminal region strongly aligns with bacterial RmlD's but also include canonical sequences found in the catalytic region of epimerases. The entire polypeptide exists as three isoforms: RHM1, RHM2, and RHM3[4].

While debate continues where exactly viruses straddle the line between living and nonliving organisms, they have not been left out of the nearly ubiquitous nature of rhamnose. For example, the nucleocytoplasmic large DNA viruses *Acanthocystis turfacea* chlorella virus 1 (ATCV-1)

and *Acanthamoeba polyphaga* mimivirus contain within their genome one or more genes coding for rhamnose biosynthetic enzymes[6]. A testament to the sometime bewildering host-pathogen relationship when viruses are involved is the probable horizontal gene transfer between the *Paramecium bursaria* Chlorella virus (PBCV-1) and its host, neither a bacterium nor a mammal, of both bacterial and mammalian genes involved in rhamnose and fucose biosynthesis[16]. PBCV-1 was the first virus confirmed to encode its own enzymes for nucleotide sugar metabolism[16]. Several years later, both ATCV-1 and mimivirus would also have similar genes annotated and the resulting enzyme activity confirmed[6]. Rhamnose can be found alongside fucose in glycosylated structural proteins such as Vp54, which contribute to virus protease resistance and antigenicity[16]. Following the production of GDP-D-rhamnose and GDP-L-fucose, the viral genome also contains the requisite genes for glycosyltransferases used to glycosylate the capsid proteins[6].

The viral pathway differs slightly from previously mentioned examples of rhamnose biosynthesis. The pathway branches into two sections, leading to GDP-D-rhamnose and GDP-L-fucose. It begins with GDP-D-mannose, the deoxy

isomer of GDP-D-rhamnose. No epimerization reaction is required, as the starting sugar moiety is mannose rather than glucose. Mannose is a C-2 epimer of glucose, hence the epimerization step is preempted by virtue of the starting sugar. Thus, only two steps are required to produce GDP-D-rhamnose, both carried out by GDP-D-mannose 4,6-dehydratase (GMD). Despite the singular name, this enzyme is bifunctional and catalyzes the NADP+ dependent dehydration, followed by the NADPH dependent reduction to form GDP-D-rhamnose. Following the first reaction by GMD, the product can also feed into the biosynthesis of GDP-L-fucose. In keeping with the remarkable efficiency of viral genomes, the enzyme GDP-4-keto-6-deoxy-D-mannose epimerase/reductase is also bifunctional and has similar functions to the bacterial RmlC and RmlD. As in bacteria with xylo-hexulose being epimerized to lyxo-hexulose, so is the mannose moiety epimerized to galactose and subsequently reduced to the end product, in this case GDP-L-fucose.

Fungi have evolved to use rhamnose in a wide variety of cellular functions. Glycoproteins, exopolysaccharides, hyphae in *Rhynchosporium secalis*, and rhamnomannans are only some examples of the rich diversity of rhamnose

utilization in fungi. Pathogenic species of fungi often include rhamnose functions including recognition and adhesion to a host. As polysaccharides, they play an important role in biofilm formation and protection against desiccation. Chestnut blight, *Cryphonectria parasitica*, secretes an exopolysaccharide with rhamnose as the terminal sugar moiety for modulating host-pathogen interactions. Nonvirulent strains of *C. parasitica* lack this exopolysaccharide. *Magnaporthe grisea*, a rice pathogen and causative agent of rice blast disease, is estimated to annually destroy enough rice to feed over sixty million people[17]. This biotrophic fungus proliferates inside plant tissues, concurrently damaging the rice and reducing yield. *Botryotinia fuckeliana* is a necrotrophic fungus which attaches to and kills its host by secretion of enzymes and toxics, invading tissues following the host's death[17]. All three of these agriculturally relevant pathogens utilize rhamnose in multiple forms during their life cycle. Also, in the human pathogen responsible for candidiasis, *Candida albicans*, rhamnose it part of polysaccharides used for biofilm formation during infection[18]. Rhamnose plays many roles

in pathogenicity among fungi. Indeed, over 200 fungi species are known to cause disease in humans.

The end product of the fungal rhamnose pathway is UDP-rhamnose, unlike bacteria where dTDP-rhamnose is the final result. In contrast to bacteria, the pathway is generally considered to being with an already charged UDP-glucose instead of with the nucleotide diphosphate being attached to glucose. UG4,6-Dh, the homologue of RmlB, carries out the dehydratase function. However, the bacterial RmlC and RmlD activity are combined onto a single, large bifunctional enzyme, U4k6dG-ER, which catalyzes both the epimerization and reduction of UDP-4-keto-6-deoxyglucose into UDP-rhamnose.

In keeping with human and agricultural interest in rhamnose, the environmentally friendly insect control agent produced by *Saccharopolyspora spinosa*, the spinosyns, are macrolides comprised of a 21-carbon tetracyclic lactone with two attached deoxy sugars: a tri-O-methylated rhamnose and forosamine, a dimethyl amino sugar derived from the rhamnose pathway[19]. Rhamnose is attached first, followed by S-adenosyl-L-methionine (SAM) dependent methyltransferases leading to tri-O-methylation at the 2′, 3′, and 4′ positions of the rhamnose moiety.

Only after the tri-O-methylation is complete is forosamine added at the 9-oxy position on the lactone. The spinosyns bind to nicotinic acetylcholine receptors and also act as γ-amino-butyric acid (GABA) neurotransmitter agonist. Insecticidal activity is by nervous system hyperexcitation.

While *S. spinosa* is a bacterium with the standard four step pathway to a nucleotide diphosphate charged rhamnose, the product of the dehydratase reaction also feeds into the spinosyn biosynthetic pathway. Gene duplication of the first two shared steps, gtt and gdh, results levels of spinosyn more than doubling[19]. This increased flux yields an increase in TDP-4-keto-6-deoxy-D-glucose, the rate limiting substrate in both pathways. The excess not needed for cell wall production is utilized in increasing the production of spinosyns. By incorporating additional copies of gtt and gdh, the commercial yield greatly increased. This yield increase facilitates the usages and financial viability of the spinosyns, which having the benefits of high efficacy, a broad insect pest spectrum, low toxicity in mammals, and a relatively safe environmental profile.

The specific purpose, and whether that purpose is essential, correlates with the positioning of the four *rml* genes within the bacterial genome. In *Escherichia coli*, rhamnose is used as one of three sugar moieties in lipopolysaccharide[20]. While critical for infection, defects in dTDP-rhamnose biosynthesis are not lethal here. However, *Streptococcus pyogenes* has an absolute requirement for rhamnose in the production of over half of its cell wall. We observe in *E. coli* that the four genes are located adjacently in the same operon in the order B, D, A, C. *Pseudomonas aeruginosa* also displays the same gene adjacency and B, D, A, C order, with rhamnose again playing an important but non-essential role in glycolipid biosurfactant and lipopolysaccharide biosynthesis[21]. Again, rhamnose's usage is necessary for infection but not survival. This positioning within the same operon and the same order is common in bacteria without a survival requirement for rhamnose production. In bacteria where it is an essential saccharide, the gene locations are typically dispersed throughout the genome. The *rml* genes in *S. pyogenes* have no obvious relationship to one another through genome placement. For example, *rmlC* and *rmlD* are located over 130,000 bases away from one another. While

epigenetic relationships are possible, none have been discovered to date. Of interest to note is that while sequence identity between the enzymes, such as RmlC, in *E. coli* and *S. pyogenes* is not particularly high, 29%, the sequence similarity is 58.6%. While the gene sequence and genome position vary considerably within bacteria, the amino acid sequence is functionally highly similar and crystal structures solved to date show little variation between species. As dTDP-rhamnose is the end product of the bacterial pathway regardless of the cellular destination of rhamnose, this is not unexpected.

Species of the *Mycobacterium* genus, from *M. marinum* to *M. abscessus* to the infamous *M. tuberculosis*, utilize rhamnose as a saccharide linker between peptidoglycan and galactan moieties of the arabinogalactan layer[13]. This is a unique feature of *Mycobacteria*. While bacteria across genera use, and in some cases require rhamnose, only *Mycobacteria* are known to utilize rhamnose to tether two layers of the cell wall together. While classified as Gram-positive, *Mycobacteria* contain features of both Gram-positive and Gram-negative bacteria. Focusing on *M. tuberculosis*, the cell envelope is composed of three major components[22]. From the exterior inward, the waxy

capsule-like material, the mycolic acid-arabinogalactan-peptidoglycan complex (MAPc), and the plasma membrane create a unique envelope that is highly resistant to both environmental stressors and antibiotics[23].

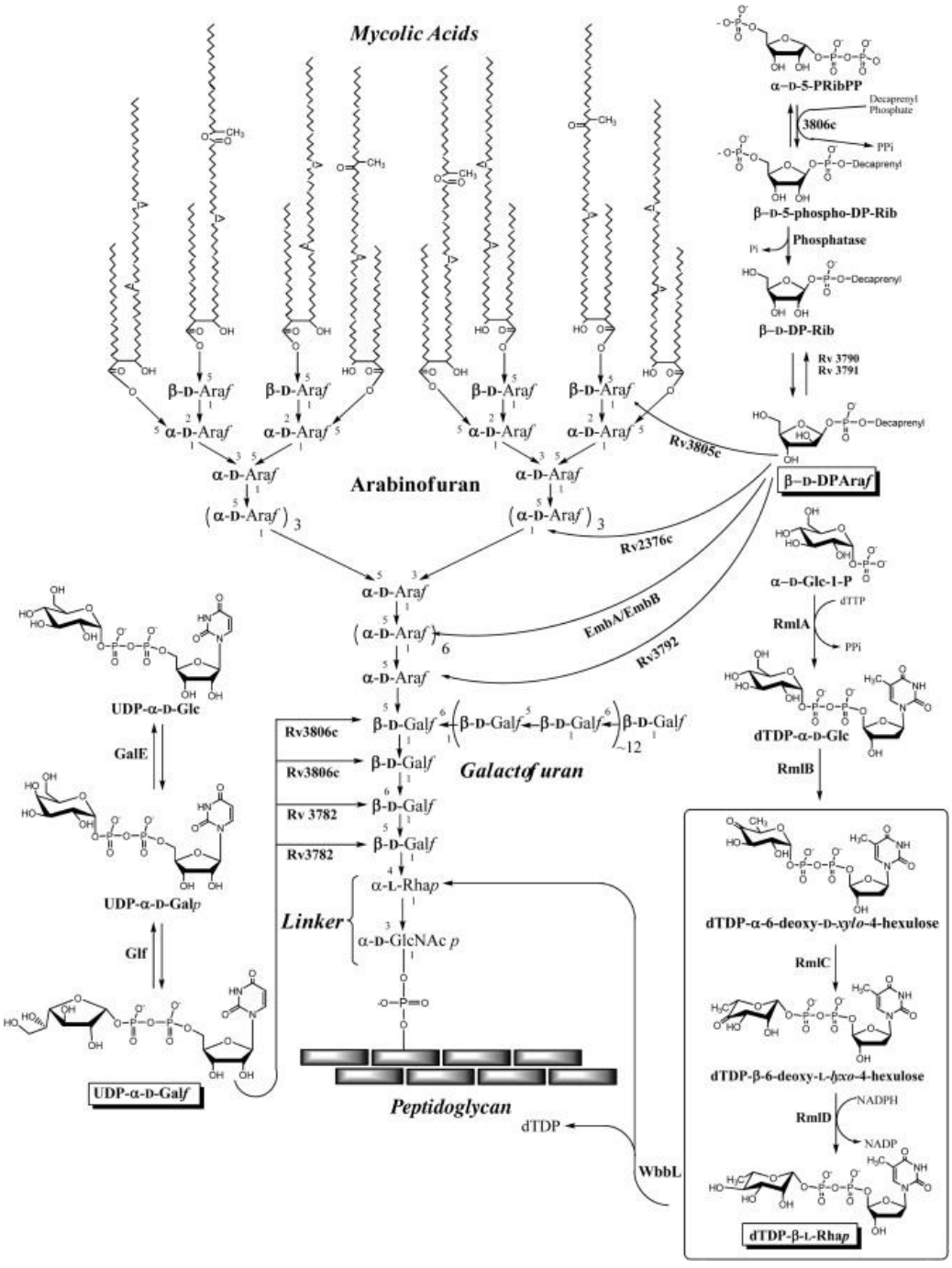

Figure 2: Diagram of *M. tuberculosis* cell wall[1]

Reproduced with permission from publisher Elselvier, license #4472791452802, Sivendran et al, 2010

Mycobacterium tuberculosis is a particularly ubiquitous infective agent, with an estimated one-third of the population currently colonized by it[24]. Fortunately for humans, most of those infected will remain carriers and never progress to an active infection. However, the large number of infected still leads to an average of over one million deaths a year[25]. A variety of factors, from being among the slowest growing of bacteria to a cell wall acting as a waxy barrier to antibiotics and environmental stressors, making this pathogen particularly difficult to treat[26]. It is mostly found in the eastern hemisphere, with emphasis on Sub-Saharan Africa. A complicating factor in treating tuberculosis is that a treatment regimen will last several months, creating issues with both patient compliance and cost. A latent infection is generally treated with isoniazid or in combination with rifampicin[27]. An active infection requires a more aggressive approach, with up to several antibiotics being combined to increase efficacy and to reduce the risk of developing antibiotic resistance.

The genetics of *M. tuberculosis* rhamnose biosynthesis follow the "essential" model, with the four *rml* genes being found in multiple loci having no obvious

relationship to each other. Each gene is a single, non-redundant copy. As expected, the *rml* genes of *M. tuberculosis* are considerably similar to other species such as *E. coli*, P. *Aeruginosa*, and *S. pyogenes*.

The MAPc is comprised of cross-linked peptidoglycan, covalently bound to arabinogalactan chains via phosphoryl-N-acetylglucosaminosyl-rhamnosyl units. α-alkyl and β-hydroxy mycolic acids are esterified to the non-reducing ends of arabinan[28]. The biosynthesis of this complex realizes the convergence of many different pathways, including the non-mevalonate pathway for isoprenoid production. Starting with peptidoglycan, uridine diphosphate N-acetylglucosamine is converted through a six step process into uridine diphosphate N-acetylmuramic acid (MurNAc) pentapeptide. The isoprenoid undecaprenyl phosphate is produced through a six step process beginning with the condensation of pyruvate and glyceraldehyde-3-phosphate. Undecaprenyl phosphate acts as a membrane acceptor, receiving the phospho-MurNAc-pentapeptide moiety of UDP-MurNAc-pentapeptide to create Lipid I. The addition of GlcNAc to the MurNAc residue of Lipid I leads to Lipid II, which is comprised of the completed disaccharide-peptide monomer unit: GlcNAc-β-(1→4)-MurNAc-l-Ala-γ-d-Glu-

A2pm (or l-Lys)-d-Ala-d-Ala. Lipid II is carried by the ABC transporter enzyme flippase through the hydrophobic core of the cytoplasmic membrane to external sites for polymerization. The two major types of modifications are the formation of glycan chains by glycosyltransferases and crosslinking by transpeptidases, which also bind it to the preexisting peptidoglycan.

The biosynthesis of the arabinogalactan layer begins with the transfer of GlcNAc-1-phosphate from UDP-GlcNAc to the terminal prenyl phosphate of peptidoglycan[29]. The terminal glucosamine is then rhamnosylated, forming the linker region between peptidoglycan and arabinan. This rhamnose residue is produced from a four step pathway, followed by the Wbbl-catalyzed rhamnosyl transferase reaction to link it to the glucosamine.

The dTDP-rhamnose is the charged form of rhamnose used for the rhamnosylation reaction. The pathway begins with the enzyme RmlA, functioning as a D-glucose-1-phosphate thymidylyltransferase[30]. RmlA transfers deoxythymidine phosphate from deoxythymidine triphosphate to D-glucose-1-phosphate, forming dTDP-glucose. RmlB is a dTDP-D-glucose-4,6-dehydratase, catalyzing the NAD+ dependent oxidation of the C4 hydroxyl of the glucose

residue, followed by the removal of a water via dehydration and forming dTDP-6-deoxy-D-xylo-4-hexulose[31]. RmlC has no cofactor, functioning as an epimerase of the 3 and 5 positions of the xylo-4-hexulose residue. In the penultimate step, rhamnose is formed through the RmlD-catalyzed reduction of the C4 keto group of dTDP-6-deoxy-L-lyxo-4-hexulose into dTDP-rhamnose. This charged rhamnose is attached to the added terminal glucosamine of peptidoglycan, completing the linker with dTDP as a side product of the transferase reaction.

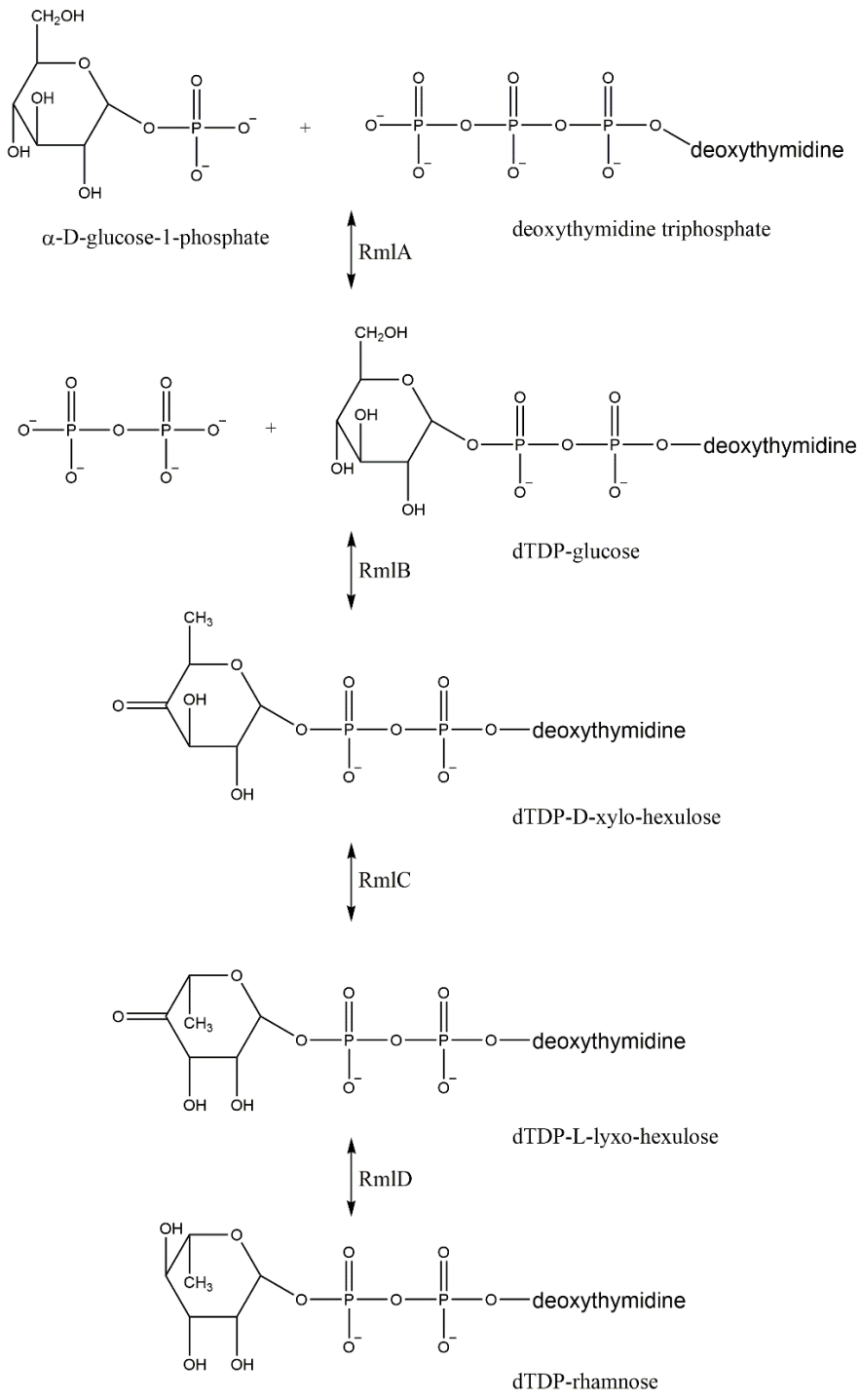

Figure 3: Representation of the rhamnose pathway

The RmlA reaction follows a sequential ordered bi bi mechanism in which the substrates bind in an obligate order, followed by the reaction and the products departing in an obligate sequence[20]. Structural studies with a bound dTTP suggest the formation of a covalent intermediate with dTMP does not occur and mechanistic experiments show the dTTP binds first[30]. This is consistent with an S_N2 type reaction, with dTTP binding to the protein, followed by glucose-1-phosphate (G1P). G1P acts as a nucleophile, attacking the α-phosphate of dTTP and the β/γ phosphates leave as pyrophosphate. The reverse reaction is possible, with the α-phosphate of dTDP-D-glucose undoing a nucleophilic attack by pyrophosphate and displacing G1P.

RmlB is a three-step mechanism, with oxidation following by dehydration and finished by reduction. Structural studies have elucidated tyrosine as beginning the reaction as a base by extracting a proton from the C4' hydroxyl on the glucosyl residue of dTDP-glucose, followed by the concomitant abstraction of a hydride by NAD+ from the C4 position. This creates the 4-ketosugar that is key to lowering the pK_a of the C5 proton, allowing for the

dehydration step to occur. An aspartate in the protonated state makes contact with the C6′ hydroxyl, donating a proton to O6 through a hydrogen bond. O6 abstracts this proton, cleaving the C6-O6 bond with water as the leaving group. The final step involves the newly formed NADH transferring a hydride back to the glycosyl C6′, causing a configuration inversion at C6 and a proton addition to C5. The deprotonated tyrosine is regenerated and dTDP-4-keto-6-deoxy-D-glucose is produced. Allard et al solving the structure of RmlB and characterizing it was paramount to determining the mechanism of the enzyme[32, 33].

The third step, RmlC, catalyzes a double epimerization at the C5′ and C3′ positions[34]. While the mechanism has not been definitively proven to date, a suggested mechanism based on structural and biochemical data suggests the C5′ position is epimerized first, although the data does not exclude the possibility of a primary C3′ epimerization. The key residues are histidine and tyrosine, with histidine acting as a catalytic base for both epimerizations and tyrosine donating a proton to the C5′ position. To prevent the energetically unfavorable C6′ O1′ diaxial and C6′-histidine clash, the sugar flips as the proton is transferred to C5′. For the second

epimerization the twisted boat conformation is most energetically favorable, with C4′ moving upward through the ring plane[35]. Histidine abstracts a hydride from C3′, leading to an oxyanion forming at C4′. The oxyanion reverts to a carbonyl following a second epimerization, forming dTDP-6-deoxy-L-lyxo-4-hexulose.

The final step is an NADPH-mediated reduction catalyzed by RmlD. This enzyme utilizes a catalytic triad of threonine and a conserved tyrosine-XXX-lysine sequence. This triad in conjunction with the presence of a Wierenga motif (glycine-XX-glycine-XX-glycine) in a Rossmann fold classifies RmlD as a member of the reductase/epimerase/dehydrogenase superfamily. The catalytic triad protonates the carbonyl and deprotonates the hydroxyl via tyrosine and threonine, respectively. The lysine bonds with the ribosyl unit of NADPH and lowers the pK_a of threonine.

All five of these reactions are essential and cannot be complemented with other enzymes in the *M. tuberculosis* proteome. Humans do not have any known biosynthetic pathway for or utilization of rhamnose. Human gut flora are known to metabolize rhamnose but no outcomes other than flatulence, increased serum propionate via uptake

from intestinal fermentation, and gut flora growth are experienced. As such, the pathway has been considered a drug target since its elucidation. Additional benefits of rhamnose targeting in *M. tuberculosis*, and all bacteria, is that rhamnose cannot be supplemented[13]. Only the charged form, dTDP-rhamnose and other nucleotide variants, can be utilized and must be produced via the *rml* pathway. As suggested by gut flora growth, bacteria can take up the rhamnose saccharide via a transporter and use it as a carbon source. However, rhamnose catabolism and dTDP-rhamnose biosynthesis are separate functions with no crossover. dTDP-rhamnose is formed from D-glucose-1-phosphate, converted from D-glucose. It is this glucose that is ultimately converted to the rhamnose residue of dTDP-rhamnose.

Each of the four *rml* genes and *wbbl* have been extensively studied to determine their essentiality. The most common method documented is the use of a chromosomal knockout of the gene in question in conjunction with a copy on a temperature sensitive plasmid. Each gene has been tested in a *Mycobacterium smegmatis* mc^2155 model, in all cases with a functional copy of the corresponding *Mycobacterium tuberculosis* homolog. In each case, the *M.*

tuberculosis gene was able to complement the loss of the *M. smegmatis* chromosomal copy. Qu et al created an *M. smegmatis* strain with a chromosomal knockout of *rmlA*, with the *M. tuberculosis rmlA* on a plasmid capable of curing when grown at 42˚C[36]. When shifted from 30˚C to 42˚C, after 24 hours cell density, as determined through A_{600}, began dropping and continued to decrease until the end of the experiment. No growth defects were observed in the comparative sample kept at 30˚C. Scanning electron microscope showed cells with severe morphological defects, including lysed cells. Li et al performed a nearly identical experiment to test for the essentiality of *rmlB* and *rmlC*. In both cases, the chromosomal copy resulted in a loss of viability which could be rescued by a *M. tuberculosis* copy on a temperature sensitive plasmid. Ma et al created the same type of experiment for *rmlD*, showing that the knockout resulted in a loss of viability. The final step for incorporation into the cell wall, *wbbL*, was also tested in Mills et al, showing lethality in absence of complementation by the *M. tuberculosis* copy[37].

In the early stages of drug development, a method to assay the activity of the target enzyme is highly

important to finding compounds with inhibitory capability. It is fortuitous that each of the four rml enzymes are soluble and active when expressed in *E. coli*. Assays have been optimized for measuring the activity of each enzyme. While substrates are commercially available for RmlA and RmlB, RmlC and RmlD must be coupled to RmlB as their substrates are either not commercially available or too unstable to synthesize. RmlC cannot be easily measured by itself, requiring the subsequent RmlD reaction to assay its activity. Initially, RmlA was measured by endpoint assays using malachite green to measure phosphate production[38]. However, real time assays are now available with the advent of a fluorescent phosphate binding protein. RmlB can be assayed by measuring NAD+ turnover. RmlC and RmlD are measured by RmlD's NADPH turnover, requiring coupling with RmlB to produce the RmlC substrate. Ma et al has developed a microtiter assay to allow for high throughput screening the terminal three enzymes, which has a strong possibility of improvements allowing the entire pathway to be screened simultaneously[39].

Indeed, assay development has led to multiple high throughput screening experiments of the rml enzymes,

resulting in novel inhibitors being discovered. Compounds with varying degrees of efficacy for each enzyme are known, although not all have been tested against the *M. tuberculosis* enzymes. Given the high degree of homology of the rml enzymes, it is not unreasonable to predict that an inhibitor of one bacterium's RmlA would have some efficacy against the *M. tuberculosis* RmlA. Alphey et al conducted a high throughput screen of the *Pseudomonas aeruginosa* RmlA and discovered nanomolar inhibitors with a scaffold based on a pyrimidinedione core[40]. These are particularly unique in that they are allosteric inhibitors with competitive inhibition curves. The structure of *P. aeruginosa* RmlA has also been solved and characterized[41]. RmlA is known to be allosterically inhibited by the pathway end product, dTDP-rhamnose, through a second binding site. Crystal structures of the inhibitors bound to the *P. aeruginosa* RmlA suggest the mechanism of inhibition is by preventing the conformational change required for the bi-bi mechanism to function[40]. Other RmlA structures further support this[42]. The allosteric site amino acids which interact with the inhibitors are identical to those found in *M.*

tuberculosis, suggesting a strong likelihood of both some level of efficacy and a similar binding motif.

RmlB has prior inhibitor screening as well in a non-tubercular bacterium, *Streptococcus mutans*. Mere months before this writing, van der Beek et al published results of a Maybridge library high through screen resulting in a few inhibitors, with one designated as a lead molecule to due to no cytotoxicity up to 15mM against U937 human monocytic cells[43]. The lead molecule, 5-(4-Chlorophenyl)-2-furoic acid, is easily obtainable and inexpensive, with its small size (222g/mol) creating possibilities for modifications while remaining amenable to the active site. The compound has only moderate micromolar efficacy against the enzyme and cells but to date is the only confirmed RmlB inhibitor published. As with RmlA, the *S. mutans* RmlB is highly similar to *M. tuberculosis* and would likely have some degree of inhibition. Crystal structures of multiple examples of RmlB have been published in other organisms[44].

The third step in the pathway, RmlC, has been considered the most ideal of the four for drug targeting due to not requiring a cofactor. Practical considerations of inhibiting an enzyme that uses a cofactor or substrate

also used by many human enzymes is a reasonable concern. RmlA's substrate is D-glucose-1-phosphate, ubiquitous in the human body. RmlB and RmlD both utilize NAD+ and NADPH, respectively. Cross reactivity with a human enzyme would pose a threat to a compound's ascension to becoming a commercial antibiotic. RmlC uses no cofactors and its substrate, dTDP-4-keto-6-deoxyglucose, has not been found in humans. RmlC was screened against a library of over 200,000 compounds by Sivendran et al, yielding a new class of inhibitors[1]. The triazinoindol-benzimidazolones have remarkable efficacy against *M. tuberculosis* RmlC, with the most potent analog having an IC50 of 120 nM[1]. The MIC against cells is calculated to be 9µg/ml, putting it close to the commercial antibiotics rifampin and ethambutol. Cytotoxicity testing against human aortic endothelial (HAE) cells yielded an IC50 of 75µM. Only a single analog was tested against HAE cells, so it is unknown if the other analogs would display a lower cytotoxicity. Regardless, this is an impressive beginning to determining the viability of RmlC as a candidate for an antibiotic. The indole ring is a well-documented moiety in many biologically active natural and synthetic products, with a wide range of therapeutic targets, such as anti-

inflammatories, HMG-CoA reductase inhibitors, phosphodiesterase inhibitors, and cannabinoid receptors agonists.

The final enzyme in the pathway in *Mycobacterium tuberculosis*, RmlD, has benefited from a virtual screen of a library. In addition, the structure of RmlD in other organisms offers a homology model for this screening[45]. Wang et al conducted a virtual screen of a 140,000 compound library to probe for inhibitors[2]. As the *M. tuberculosis* RmlD structure was not known, a homology model using the *Salmonella enterica* serovar Typhimurium structure. Again, the high degree of conservation across species has proven a boon for drug design. Structure-based drug design has long been a process for developing new antibiotics by comparing the activity of compounds which are similar in structure but through slight differences provide considerable data for future alterations[46]. Compounds with favorable predicted binding energies were funneled through multiple levels of additional screening, such as modeled interactions with essential active site residues with the idea resistance would be less likely to develop. Following this, compounds underwent a final round of screening to ensure they conform to Lipinski's rule of

five, which states: no more than 5 hydrogen bond donors, no more than 10 hydrogen bond acceptors, a molecular mass less than 500 daltons, and a logP/ClogP not greater than 5[47]. They are a rule of thumb regarding the "drug-likeness" of a compound. The final four compounds are structurally similar, with three being analogs of each other. The results were encouraging with a caveat. While the two most potent compounds enzymatically had IC50's as low as the nanomolar range, they had only moderate efficacy against whole cells. The other two compounds had excellent efficacy against whole cells, but were only moderate enzymatic inhibitors. It would not be unreasonable to suggest this could be reconciled through crystal structures and synthetic chemistry, resulting in a compound with excellent enzymatic and ultimately high whole cell potency.

By far the most common antibiotic class used to treat infections is the β-lactam, which until 2003 accounted for over half of antibiotic sales in the world[48]. While molds have anecdotally been observed to inhibit bacterial growth and even used to treat wounds, it was not until Alexander Fleming serendipitously discovered penicillin in 1929 that β-lactams began their advent to becoming the

world's leading antibiotic[49, 50]. After years of investigation it was discovered that β-lactams target peptidoglycan biosynthesis in bacteria, the mesh-like layer in the cell wall found in all known bacteria except for the families *Chlamydiaceae* and *Mycoplasmataceae*[51-53].

The general structure of a gram-positive bacterial cell wall is an inner membrane surrounded by a layer of peptidoglycan, with gram-negative bacteria having a thinner peptidoglycan layer with an outer membrane. The peptidoglycan layer varies in thickness, with gram-positive bacteria having a much thicker layer comprising half or more of the cell envelope while only comprising about 10% of gram-negative cell envelope. The larger amount of peptidoglycan in gram-positive bacteria allows for the eponymous gram staining technique to distinguish them from gram-negative bacteria through crystal violet and iodine forming a complex within the framework, preventing the dye from washing out. *Mycobacterium tuberculosis* is unique in that the amount of peptidoglycan in its cell wall would place it squarely within gram-positive, however it does not readily stain due to a thick, waxy layer of mycolic acids on the exterior of the

cell wall preventing the dye from entering the cell. Instead, when *M. tuberculosis* is suspected an acid-fast stain such as Ziehl-Neelsen or fluorescent stain such as auramine is used.

As with any layer in the cell wall, major disruption of this peptidoglycan layer is invariably lethal. In addition to influencing the shape of the bacterium, peptidoglycan also provides protection against sheering forces and osmotic stress. The aptly named penicillin-binding proteins (PBPs), the targets of β-lactams, are the penultimate architects of this framework by at least two of three mechanisms: D-alanine carboxypeptidase, peptidoglycan transpeptidase, and peptidoglycan endopeptidase. The enzymes have bifunctionality, with an N-terminal transglycosylase domain involved in the formation of linear glycan strands and a C-terminal transpeptidase domain involved in cross-linking of the peptide subunits that is the target of β-lactams. An active site serine is conserved in all members of the PBP family.

Given the ancient biological origins of β-lactams, it is unsurprising that an evolutionary arms race has continued unabated since certain species of fungi began

attacking bacteria. Bacteria have responded with their own defensive molecule, the enzyme β-lactamase. The suffix eloquently reveals the function: breaking down β-lactams. These enzymes catalyze the hydrolysis of the namesake chemical moiety, the β-lactam ring. This four-membered cyclic amide is an essential component of this antibiotic class and upon hydrolysis, is rendered ineffective. Bacteria expressing β-lactamases thus have an evolutionary advantage over other bacteria when encountering β-lactam-producing fungi. The genes coding for these enzymes have been sequenced and bear a degree of similarity to PBPs such that they are hypothesized to have evolved from them. Indeed, one can follow the trail of crumbs to this conclusion. By simply comparing the structure of penicillin to the D-alanine-D-alanine terminus of the transpeptidase substrate, a remarkable structural mimicry becomes obvious.

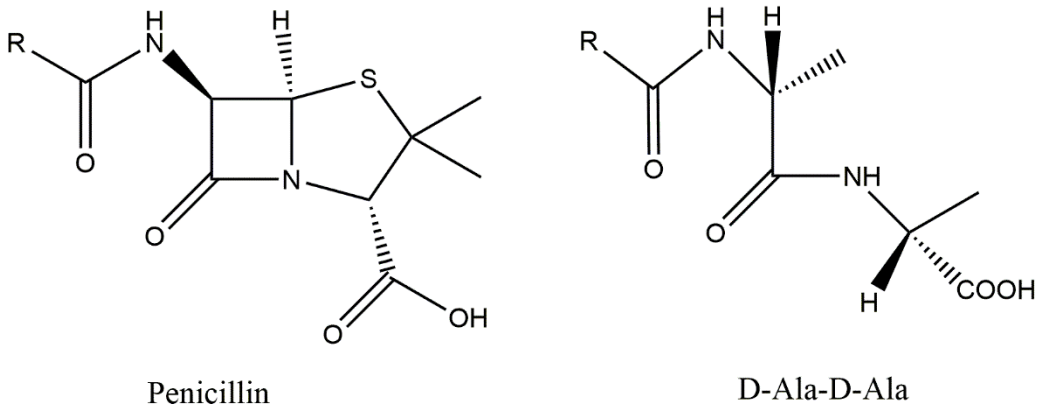

Figure 4: Mimicry between penicillin and D-ala-D-ala

Structural comparison of Penicillin with the substrate of the transpeptidases targeted by penicillin

It follows that an enzyme evolved from a PBP would retain a similar level of substrate recognition. A non-essential enzyme with the same type of substrate recognition as a PBP could then serve as a defensive line, binding to β-lactams in lieu of them inhibiting the PBPs. Indeed, β-lactamases are often secreted to hydrolyze β-lactams before they can enter the cell. This insult has not been unchallenged, with evolution resulting in clavulanic acid from *Streptomyces clavuligerus[54]*. Clavulanic acid has negligible bactericidal activity but is able to act as a suicide inhibitor against many β-

lactamases. Upon covalently binding to the active site serine, a rearrangement occurs and creates a more reactive imine. This imine can follow two paths. The first involves the imine stabilizing upon tautomerization to an enamine, resulting in a transient inhibition. The second path occurs when a second active site nucleophile is acylated by the imine, resulting in a cross-linked enzyme, leading to irreversible inactivation. As such, clavulanic acid is co-administered with a bactericidal β-lactam. In addition to increasing the efficacy of the bactericidal activity of the other β-lactam, this also allows for antibiotics that previously had limited use against resistant bacteria to become effective again and permits safer and less costly antibiotics to be used.

Mycobacterium tuberculosis is renowned for being able to evade β-lactams due to its promiscuous broad spectrum class A β-lactamase, BlaC. To date, there is no FDA approved β-lactam for treating tuberculosis. Much research over the years has been conducted on BlaC in an attempt to understand how it is able to readily hydrolyze approved β-lactams, including the first crystal structure by Wang et al in 2006[55]. Upon structural elucidation is became apparent that the flexible substrate specificity loop

allowed the active site to accommodate β-lactams of varying size and shape. Recent advances have shown the newer penem and carbapenem classes of β-lactams have clinical relevance and have gained approval in other countries such as Japan.

Another pathogenic bacterium known for its ability to shrug off antimicrobials is the Gram-negative *Pseudomonas aeruginosa*. Particularly noteworthy is that, while individual strains vary in susceptibility to different antibiotic classes, only the fluoroquinolone class is generally effective against all strains. However, fluoroquinolone-resistant strains are increasing in frequency in clinical settings. The low antibiotic susceptibility is widely attributed to the presence of multidrug efflux pump genes (i.e. *mexAB*, *mexXY*) and the low permeability of the cell wall. *P. aeruginosa* is also capable of rapidly acquiring resistance through horizontal gene transfer and chromosomal mutations. Biofilm formation further restricts the uptake of antibiotics. Cystic fibrosis (CF) patients are particularly vulnerable to *P. aeruginosa* infection and this pathogen is the single largest contributor to CF patient mortality[56].

Pseudomonas aeruginosa is a Gram-negative bacterium capable of infection plants and animals. Diagnostic tests categorize it as citrate, catalase, and oxidase positive. A hallmark characteristic of *P. aeruginosa* is the blue-green color most strains exhibit from pyocyanin and pyoverdine biosynthesis. Pyocyanin is an important virulence factor, capable of generating reactive oxygen species. Strains defective in pyocyanin biosynthesis exhibit a marked decrease in the ability to initiate an infection. Pyoverdine is able to assist in the uptake of iron from the extracellular environment and mediates exotoxin A. It is a facultative anaerobe, capable of using nitrate and nitrite as a terminal electron acceptor. While found virtually everywhere in the environment, *P. aeruginosa* is more an opportunistic pathogen and is more common among the young, old, and otherwise physiologically compromised patients. It is especially known for a high degree of morbidity among cystic fibrosis patients.

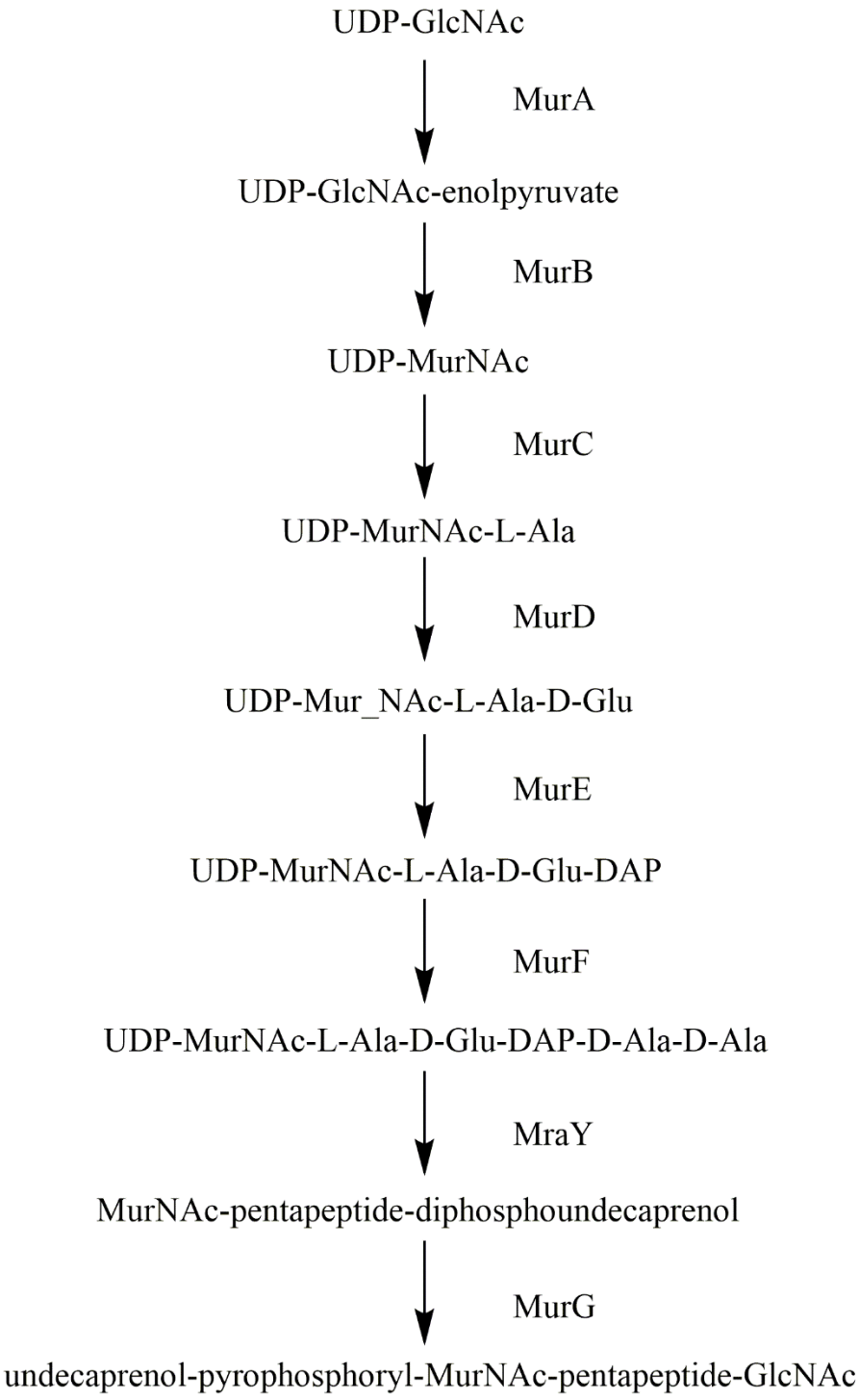

Figure 5: Representation of the Mur pathway

The Mur pathway is the first committed step to peptidoglycan biosynthesis, with MurA through MurF resulting in the UDP-MurNAc-pentapeptide followed by MraY and MurG to produce Lipid I and Lipid II, respectively[57]. The first six steps are comprised of MurA, a transferase, MurB, a reductase, and the four ATP-dependent ligases, MurC-MurF. They are all highly conserved across bacterial
species and possess no counterparts in eukaryotes, who lack peptidoglycan. Each gene is a single copy and generally found in separate operons.

This study will primarily discuss the first step, MurA, in *Pseudomonas aeruginosa*. Denoted as UDP-N-acetylglucosamine 1-carboxyvinyltransferase (EC 2.5.1.7), MurA catalyzes the transfer of the enolpyruvate moiety of phosphoenolpyruvate (PEP) to the 3’-OH hydroxyl group of UDP-GlcNAc, resulting in phosphate as leaving group[58]. In a deviation from the expected use of the high energy P-O bond of the phosphate in a reaction involving PEP, the C-O bond is instead cleaved. The mechanism entails an “induced fit” in which UDP-GlcNAc must bind MurA before PEP[59]. The reaction follows an addition-elimination course in which the enzyme-substrates complex forms an

intermediate state where the two substrates are covalently linked with the PEP C-2 assuming a tetrahedral configuration and C-3 becomes a methyl group. The resulting carboxyvinyl ether forms the starting point for the addition of the five amino acids in the terminal pentapeptide following MurB-MurF, resulting in UDP-MurNAc-pentapeptide. It is not uncommon for the first committed step of a pathway to be feedback inhibited by later products. Indeed, *E. coli* MurA is inhibited by the product of MurB, UDP-MurNAc. Given the high degree of similarity between MurA enzymes, it can be predicted that other species would face the same feedback inhibition. *murA* was confirmed in 1995 to be essential following a chromosomal deletion in conjunction with an arabinose inducible plasmid containing a copy of *murA*. Growth of cells containing the *murA* deletion was dependent on the presence of arabinose to induce expression of *murA* from the plasmid.

The phosphate produced by the reaction initially left the assay amenable only endpoint monitoring by malachite green[38]. Toxic by itself, the malachite green must then be activated by sulfuric acid. Fortunately, advances have created methods to assay MurA in real time and without

dangerous chemicals. Two modern methods include a purine nucleoside phosphorylase which utilizes the inorganic phosphate to split the bond between the phospho-ribose sugar and the nucleoside, allowing for monitoring at 360 nm[60]. The second method uses a synthetic phosphate-binding enzyme, which fluoresces upon binding.

Following the production of UDP-MurNAc-pentapeptide, the membrane stage of peptidoglycan biosynthesis begins with MraY[61]. It catalyzes the transfer of MurNAc pentapeptide from UDP-MurNAc-pentapeptide to the plasma membrane-bound lipid carrier undecaprenol phosphate to form Lipid I. Lipid II is formed following the addition of a terminal GlcNAc residue. MurJ is a recently discovered flippase which carries Lipid II through the plasma membrane, “flipping” it to face the exterior of the cell.

Upon reaching the periplasm Lipid II splits into undecaprenol, which is recycled for future Lipid I production, and the GlcNAc-MurNAc-pentapeptide (GM-PP) begins the steps to integrate into the peptidoglycan framework[61]. A glycosyltransferase catalyzes the polymerization of the GM-PP to the nascent peptidoglycan chain, with a DD-transpeptidase attaching the new chain to the sacculus. The pentapeptide is trimmed by DL-, DD-, and

LD-carboxypeptidases, with DD- and LD-endopeptidases cleaving crosslinks. These cleavages allow the existing peptidoglycan to incorporate the new residues. The three LD-transpeptidases catalyze the formation of 3-3 peptidoglycan cross-links, attachment of the outer-membrane lipoprotein, and binding D-amino acids.

These insertions by themselves would only thicken the sacculus without elongating it. The growth of peptidoglycan must occur in a way that maintains a consistent thickness, else the bacteria would enlarge without end[62, 63]. A series of hydrolases, which combined are capable of cleaving nearly every physiological glycoside and amide bond, cleave peptidoglycan such that new residues can insert without increasing the thickness of the sacculus. A highly controlled regulatory framework exists, whereby peptidoglycan biosynthesis and hydrolysis is regulated by having the machinery form loosely-bound multienzyme complexes. This ensures minimal hydrolase activity except where biosynthetic enzymes are also present. These same hydrolases are indirectly involved in the activity of β-lactams. With the balance between building and hydrolysis, the inhibition of the transpeptidases by a β-lactam

results in the scales tipping to hydrolysis and result in a breakdown of the peptidoglycan framework. Knockouts of individual hydrolases show no lethality, however this can result in an altered morphology as each hydrolase has a specific bond it cleaves.

As would be expected of such a large portion of the cell wall, peptidoglycan biosynthesis is regulated in by connections multifactorial. Chief among them is cell growth and division. FtsZ is a tubulin-like protein which is a major regulator of bacterial cell division and forms a ring around the midcell designated the Z ring before cell division. Enzymes involved in Lipid II and peptidoglycan biosynthesis are recruited to the Z ring. When cell division begins FtsZ constricts at the septum, causing local stretching of the sacculus. This force promotes peptidoglycan biosynthesis at the septum where the two daughter cells separate

Targeting peptidoglycan is not the domain held solely by β-lactams. First discovered in 1969 from a soil culture of *Streptomyces fradiae*, the antibiotic fosfomycin acts as a suicide inhibitor of the enolpyruvyl transferase at the beginning of the peptidoglycan biosynthesis pathway, MurA. Fosfomycin contains an epoxide, a three atom cyclic ether,

that is strained and thus highly reactive. Confirmed through a crystal structure, it irreversibly alkylates the active site cysteine 115, inactivating MurA. Despite this high level of reactivity, fosfomycin is excreted in the urine unchanged. This suggests a considerable degree of specificity and little or no cross-reactivity with other enzymes. As it is primarily excreted in the urine in an unchanged state, this concentrates fosfomycin in the bladder and makes it a common prescription for treating urinary tract infections. It is so well tolerated by patients that it is often given as a "megadose", allowing the simplest possible regimen for high levels of compliance. It has been successfully explored as a fosfomycin/tobramycin combination inhalation therapy for CF patients[64]. These characteristics have led to it being evaluated for treating infections not previously considered.

Fosfomycin is not an outlier in the evolution of resistance mechanisms. *P. aeruginosa*, and other bacteria such as *Klebsiella pneumoniae*, express the enzyme FosA. FosA is a metal-dependent transferase that catalyzes the conjugation of glutathione to fosfomycin. This inactivates the drug. One could liken this to the activity of a β-

lactamase, as enzyme-catalyzed antibiotic degradation. The multidrug efflux pumps are able to remove fosfomycin from the cell. The active site of MurA is very large in order to accommodate both UDP-NAc and phosphoenolpyruvate, leading one to believe a mutation is unlikely to prevent such a small (138 g/mol) molecule from entering. The active site cysteine is an important catalytic residue. However, this cysteine can mutate to an aspartate, rendering the mechanism of fosfomycin ineffective. The fitness cost is minimal, with the aspartate able to take over cysteine 115's role in product release. Indeed, *Mycobacteria* and *Chlamydia* commonly have this variation innately and fosfomycin is not effective in treating those infections. The uptake of fosfomycin is also a subject of resistance mutations, with the glycerol-3-phosphate transporter glpT required for its introduction into the cell. glpT possesses relatively low specificity, able to readily transport very small (<200 dalton) molecules possessing a phosphate or phosphate mimic, including aresenate, inorganic phosphate, and fosfomycin. *P. aeruginosa* is known to develop mutations in glpT, preventing the uptake of fosfomycin. Between multidrug efflux pumps, FosA, MurA cysteine 115 mutations, and glpT,

P. aeruginosa is well equipped to meet the challenge of fosfomycin specifically and antibiotics in general.

Fosfomycin remains an effective treatment in certain circumstances but alternative inhibitor types that are not affected by FosA or the active site cysteine mutation present an attractive option. Many variations of fosfomycin have been evaluated but none have been approved for clinical use. MurA is a well validated target and offers possibilities beyond cysteine modification, which carries the potential risk of cross-reactivity. Terreic acid is a natural product from the fungus *Aspergillus terreus* that is able to covalently modify cysteine 115 and inhibit the reaction[65]. However, overexpression of MurA protected *E. coli* against fosfomycin but not terreic acid, suggesting that the antimicrobial effect of the compound is due to hitting multiple targets[66]. Alternate routes to inhibiting MurA activity such as a competitive inhibitor or a substrate mimic that can enter the pathway via MurA and inhibit thusly. Examples of both have been discovered, including an unusual compound which suspends the induced fit mechanism and obstructs the transition from an open to closed form.

The tuliposides and tulipalins are derived from tulip anthers in the families Liliaceae and Alstroemeriaceae. An acidic environment results in the conversion of a tuliposide to its respective tulipalin and is speculated that the acidis organelles of the tulip anthers catalyze this conversion upon tissue damage by a microbial attack. The tulipalins mimic phosphoenol pyruvate and are able to form a MurA-catalyzed adduct with UDP-GlcNAc, resulting in a product nearly identical to the normal product, UDP-GlcNAc-enolpyruvate[67]. It would not be unreasonable to suspect that this adduct generates a negative downstream effect such as inhibiting MurB. Chemical synthesis of these compounds has allowed for their production in house as opposed to the more laborious extraction from plant matter[68-70].

Another example of Nature's genius is the molecule cnicin, from *Cnicus benedictus*. A sesquiterpene lactone containing a phosphoenolpyruvate mimic, it is able to enter MurA and in an enzyme-catalyzed reaction, form an adduct with UDP-GlcNAc to mimic the product[71]. Unfortunately, cnicin exhibits considerable toxicity to human monocytes through an as yet unknown mechanism[72].

Chapter II of this study will detail the four dTDP-rhamnose biosynthetic enzymes in *Mycobacterium tuberculosis*, with emphasis on RmlC. Known *M. tuberculosis* rml inhibitors will be further evaluated, including crystal structures, cytotoxicity studies, and a murine pharmacokinetic model. New inhibitors against M. tuberculosis rml enzymes will be detailed. At the beginning of each chapter there will be a short background more specifically related to the respective project.

Chapter III of this study will focus on the *Pseudomonas aeruginosa* MurA, focusing on crystallographic evaluation of the enzyme with regard to substrate, product, and inhibitors of various classes. While MurA has been highly characterized in other organisms, the pseudomonal enzyme has had no structural studies published to date and only some enzymatic assessments. The efficacy of these various classes of inhibitors was also tested against *P. aeruginosa* strain PAO1.

CHAPTER II

STRUCTURAL AND FUNCTIONAL INSIGHTS INTO dTDP-RHAMNOSE BIOSYNTHETIC ENZYMES AND THEIR INHIBITION BY TRIAZINOINDOL-BENZIMIDAZOLONES

OVERVIEW

The *Mycobacterium tuberculosis* cell wall contains targets to several FDA approved antibiotics and continues to be evaluated for viability of as yet unutilized targets. The rhamnose biosynthetic pathway yields a product which forms the critical junction between the peptidoglycan and outer cell wall. Each of the four steps have been determined to be essential in *Mtb*. Sivendran et al discovered via high throughput screening a new class of molecules, the triazinoindol-benzimidazolones, that are highly effective against the third step, rmlC, and whole cells. A docking analysis was performed yielding two theoretical conformations. We have taken this class of compounds and further expanded the analysis with cocrystal structures, elucidating the exact mode of binding and offering insight into the potency or lack thereof with variations in R-groups. To test the viability of the

triazinoindol-benzimidazolones as potential antibiotics, we have evaluated the entire series for cytotoxicity against human dermal fibroblasts. Additionally, we have assessed the lead compound within the triazinoindol-benzimidazolones for kinetic solubility, plasma stability, plasma protein binding, and with hepatic microsomes. Finally, our lead compound has been given orally and intraperitoneally in a murine model to assess for bioavailability.

INTRODUCTION

dTDP-rhamnose biosynthesis in *Mycobacterium tuberculosis* presents an as yet untested target pathway in an animal model or clinical setting. β-lactams, vancomycin, capuramycin, D-cycloserine and isoniazid all target different points of cell wall biosynthesis[73, 74]. With the increasing spread of multi-drug resistant *M. tuberculosis*, scientists the world over are simultaneously researching drug targets in an attempt to outpace evolution. Previous studies reveal each of the four steps are individually essential to the survival of M. tuberculosis[13, 36, 75]. This suggests that targeting the

rhamnosyl linker between peptidoglycan and arabinogalactan may prove fruitful in developing a novel antibiotic for real world use.

The third step, rmlC, is considered the most ideal target in the pathway due to the distinctiveness of the substrate from anything found in the human body and that it requires no cofactors, which would theoretically result in a decreased likelihood that a compound would disrupt a human enzyme that utilizes a shared cofactor through an interaction with the cofactor binding pocket[76].

Triazinoindol-benzimidazolones inhibit rmlC through a competitive partial substrate/product mimicry, adopting the same pi-pi interaction with Tyr138 that exists between Tyr138 and the thymine moiety in the substrate and pathway end product. However, rather than interacting with the deeper catalytic residues in the active site the triazinoindol-benzimidazolones sit at the mouth of the active site.

Taking the initial screening results from Sivendran, we further evaluated analogs to determine the viability of substitutions in the triazinoindol moiety[1]. We also tested the compound stability, kinetic solubility, plasma stability, and plasma binding of lead compound within the

series. In addition, bioavailability in an oral murine model and serum mean residual time in an intravenous model were measured.

The triazinoindol-benzimidazolones demonstrate remarkable stability, with no detectible degradation following a DMSO stock being stored at room temperature for one week. However, the low kinetic solubility suggested that oral bioavailability would be an issue. This was supported by results in an oral murine model showing absorption far below the determined MIC.

MATERIALS AND METHODS

Cloning, expression, and purification

Wild-type RmlA, RmlB, and RmlD were amplified from M. tuberculosis H37Rv genomic DNA using Phusion polymerase from New England Biolabs and inserted into the NdeI and XhoI sites in pET30b. Wild-type RmlC was amplified from M. tuberculosis H37Rv genomic DNA using Phusion polymerase from New England Biolabs and inserted into the NdeI and HindIII sites of pET28b. These resulted in C-terminal and

N-terminal hexahistine tags, respectively. Sequences were confirmed by Eton Bioscience.

Plasmids were transformed into the Invitrogen *E. coli* BL21 (DE3) strain. To produce the protein, the bacterial cultures were grown at 37°C at 180 rpm in LB medium until an OD600 of 1.0 was reached. Following cooling to 20°C for 60 minutes, the cultures were induced with 1.0 mM isopropyl-β-D-thiogalactoside. The cells were incubated overnight at 20°C, harvested and resuspended in lysis buffer (10% glycerol, 100 mM NaCl, 25 mM $(NH_4)_2SO_4$, 10 mM imidazole, 20mM HEPES pH 7.4, and 0.5 mM TCEP). Cells were disrupted via French Press at 20,000 PSI and the insoluble cellular material was removed by centrifugation at 15,000 rpm for 1 hour.

RmlA, RmlB, RmlC, and RmlD were purified using Ni-NTA affinity chromatography in a gravity column through multiple volumes of wash lysis buffer until eluent samples no longer produced a visible color change with Bradford protein quantification reagent, indicating washing was complete. Proteins were eluted with elution buffer (5% glycerol, 50 mM NaCl, 25 mM $(NH_4)_2SO_4$, 200mM imidazole, 10mM HEPES pH 7.4, and 0.5 mM TCEP) until eluent samples no longer produced a visible color change with Bradford

protein quantification reagent, indicating elution was complete. Samples were then concentrated using Millipore Amicon Ultra-15 centrifugal filter units and injected onto a S200 size exclusion chromatography column. Peaks corresponding to the target protein were collected and concentrated to 10 mg/mL, 8 mg/mL, 20 mg/mL and 10 mg/mL for RmlA, RmlB, RmlC, and RmlD, respectively. Individual aliquots of purified protein were stored at -80°C until needed. Cloning of RmlA was originally done with an N-terminal his-tag. However, the N-terminal his-tag resulted in an insoluble protein.

Size exclusion chromatography

The molecular weight of rmlC in solution was determined by size-exclusion chromatography using a Superdex 200 GE Healthcare 16/60 column. The column was calibrated with aprotinin (6.5 kDa), carbonic anhydrase (29 kDa), conalbumin (75 kDa), catalase (232 kDa), and thyroglobulin (669 kDa). The separation was carried out at 4°C at a flow rate of 1.0 mL/min. The calibration curve of Kav versus log molecular weight was prepared using the equation Kav= (Ve-Vo/)/(Vt-Vo,), where Ve = elution volume

for the protein, Vo = column void volume, and Vt = total bed volume. Size exclusion chromatography indicates rmlC is a protein monomer.

Crystallization

Crystallization of RmlC was based on reported conditions from Kantardjieff et al, however we were unable to reproduce diffraction quality crystals in the reported condition of 0.1 M sodium citrate buffer pH 5.5, 28% polyethylene glycol monomethyl ether 2,000 and 0.33% lauryldimethylamine N-oxide (LDAO)[76]. Conditions with varying concentrations of each component were tested until diffraction quality crystals were obtained by removing all LDAO. The reported condition produces diffraction quality crystals only when all LDAO is removed, with the final optimized condition of 0.1 M sodium citrate buffer pH 6.1 and 25% polyethylene glycol monomethyl ether 2,000.

Crystallization trials of RmlA were carried out through sparse-matrix commercial screens. Protein incubated with glucose-1-phosphate were screened against Wizard, PEG/ION, Index, and Crystal Screen. RmlA formed crystals in many conditions, with 10% PEG 8,000, 0.1 mM

imidazole pH 8.0, and 200 mM CaOAc producing rods appearing most amenable to optimization. Repeated attempts at producing RmlB crystals in the presence of NAD+ resulted in spheroids in 30% PEG 5,000 MME, 0.2 M ammonium sulfate, and 0.1 M MES pH 6.5. RmlD did not yield crystals in the screening matrices used.

However, no condition was able to produce crystals of RmlA and RmlB which produced a solvable data set upon x-ray diffraction trials. The resulting reflections were highly mosaic and unable to be processed. Initially suspected as a cryoprotectant issue, many cryoprotectants were attempted such as glycerol, PEG 400, PEG 8,000, and ethylene glycol. No improvements occurred regardless of cryoprotectant.

Triazinoindol-benzimidazolone co-crystallized rmlC crystals were soaked in mother liquor for ten minutes and flash frozen in liquid nitrogen. X-ray diffraction data was collected at our home source at Texas A&M University, College Station, TX. Data sets were processed using HKL2000[77]. Data was collected at 120 K.

Evaluation of untested triazinoindol compounds

Additional compounds containing the core triazinoindol with substitutions in the benzimidazolone group were purchased from Chembridge. In addition, one compound containing both cores but with a different substitution at the R1 position was also purchased. Attempts at cocrystallization were made for each compound. The compounds were dissolved in DMSO to 100 mM and added to 20 mg/ml rmlC protein, diluting to 1mM. After incubating 1 hour on ice, the protein-compound solution was mixed in a 1:1 ratio with the optimized crystallization condition of 0.1 M sodium citrate buffer pH 6.1 and 25% polyethylene glycol monomethyl ether 2,000. The samples were spun down at 14 krpm at 4°C for 10 minutes. Crystals formed overnight and were collected at our home source R-axis over 180 degrees with 1 degree frames. Data sets were processed using HKL2000[77].

Structure determination

Initial phases were obtained by molecular replacement using Phaser in the PHENIX suite with PDB ID 1UPI as a

search model[78]. Each data set was refined against the resulting models and iterative cycles of model building and refinement were performed with Coot 0.8.9.1 and PHENIX[79]. Further structural evaluations occurred within Chimera[80].

Plasma stability

A 40 µM stock solution of the compound was prepared in DMSO. 195 µL of mouse plasma and 195 µL of phosphate buffered saline (pH 7.4) was added to a centrifuged tube and incubated for 15 minutes at 37°C. The assay was initiated by adding 10 µL of the 40 µM stock solution to the plasma/PBS mixture. At times 0, 15, 30, 60, 90, 180, and 240 minutes a 50 µL sample was removed and added to 100 µL of cold acetonitrile. 150 µL of acetonitrile containing 1 µg/mL of Warfarin internal standard was added and the tubes vortexed and centrifuged at 14,000 rpm for 10 minutes. 100µL of supernatant was transferred to LC-MS glass vial inserts with 10 µL being used for analysis. LC-MS was calibrated using sodium formate peaks. Extracted Ion Chromatogram was used to find the target and Warfarin peaks, with a ratio of mass areas to Warfarin calculated

for all time points. The percentage of the parent compound loss was calculated over time.

Plasma protein binding assay

A 1 mg/ml stock solution of the compound was prepared in DMSO and diluted with mouse plasma to a final concentration of 10 µg/ml. Clozapine (high binding) and fluconazole (low binding) are used as experimental controls. The mixture was incubated at room temperature for 15 minutes, after which 300 µL of phosphate-buffered saline was added to the white wells and 100 µl of the plasma-compound mixture was added to the red wells of a Thermo Scientific Rapid Equilibrium Dialysis plate and sealed with clear film. The plate was incubated at 37°C for 5 hours at 250 rpm. 50 µL from each red and white well were pipetted into separate centrifuge tubes. 50 µL of fresh plasma was added to the buffer sample and 50 µL of PBS to the plasma sample. 200 µL of fresh acetonitrile containing 1 µg/ml Warfarin was added to each tube. 200 µL of freshly prepared water containing 0.1% formic acid was added to each tube and vortex. Tubes were centrifuged at 14,000 rpm for 10 minutes. 200 µL of the supernatant were

transferred to LC-MS autosampler vials with a 10 µL injection. The LC-MS was calibrated using the sodium formate peaks. Using an extracted ion chromatogram, the mass area of the compound and Warfarin were determined in each sample.

Then,

$$\%\, Bound = \frac{(Pl - Bu)}{Pl} \times 100$$

Where, Pl = Ratio of mass intensities of the compound and Warfarin in the plasma compartment

Bu = Ratio of mass intensities of the compound and Warfarin in the buffer compartment

$$\%\, unbound = 100 - \%\, Bound$$

Internal standards clozapine and fluconazole should have approximately 94% and 9% bound, respectively.

Kinetic solubility assay

A 5 mM stock solution of the compound was prepared in DMSO. 10 µL of the stock solution was added to 490 µL of filtered 0.1 M sodium phosphate buffer, pH 7.4, into a well on a deep 96 well polypropylene plate. A stir bar was

added to each well and let spin for 24 hours at room temperature at approximately 4 rpm. After 24 hours, the plate was centrifuged at 1,000 x G for 1 minute. 20 µL of supernatant was added to 180 µL of phosphate buffer in an LC-MS autosampler vial. To prepare for single point calibration, 10 µL of the stock solution was added to 490 µL of methanol. From this solution, 20 µL were removed and added to 180 µL of methanol in an LC-MS autosampler vial. The LC-MS was calibrated using the sodium formate peaks. After running samples and standards, the mass area of the compound was determined in both buffer and methanol samples using an extracted ion chromatogram. Assuming the mass area of the methanol sample to be 100%, the percent solubility was calculated using the below equation.

$$\frac{Compound\ Mass\ Area\ (Buffer)}{Compound\ Mass\ Area\ (Methanol)} \times 100 = solubility\ (uM)$$

Mycobacterium tuberculosis whole cell assays

Analogs of the reported compounds were tested against MC^{2}7000 *Mycobacterium tuberculosis*. In addition, compounds reported for rmlB and rmlD, and new analogs, but without whole cell data were also tested. A starter culture of

cells were grown at 37°C in 7H9 media containing 0.5% dextrose, 0.08% sodium chloride, 0.05% tyloxapol, 0.25 µg/ml malachite green, and 50 µg/ml pantothenate. An aliquot of cells was then diluted in 40 ml of the same media to an OD^{600} of 0.05. 200 µL of cells were added to sterile 96 well plates. Compounds dissolved in DMSO were added in a gradient to cells, with rifampin serving as a negative control and DMSO serving as a positive control. After seven days, 4ul/well of 0.2mg/ml Resazurin is added. Following an additional 24 hours of incubation, fluorescence values are determined on a Polarstar Omega plate reader at excitation 544 nm and emission 590 nm. Cell viability is determined as a percentage of the positive control.

Human dermal fibroblast cytotoxicity assay

Human dermal fibroblasts (HDF) at a density of 64,000/mL were plated in 384-well plates at 40µL/well with a final DMSO concentration of 0.25% and allowed to incubate for 4 hours. Test compounds were added to the wells containing cells at appropriate dilution concentrations. After incubation for 24 hours, Resazurin

was added to the wells and further incubated for an additional 24 hours. The plate was then read using fluorescence intensity (excitation 530 nm; emission 590 nm). Results were graphed using Graphpad Prism version 8.0.0.

Bioavailability measurements in a mouse model

Six-week old female ND4 Swiss Webster mice (~20 g each) (Envigo, Indianapolis, IN) were used for pharmacokinetic studies. For oral administration compounds were formulated in 5% DMSO, 95% canola oil and administered as a single 100 µL oral gavage at 10 mg·kg-1. For intravenous administration, compounds were formulated in 20% Captisol® (CyDex Pharmaceutical, INC) aqueous solution and administered as a single 100 µL retro orbital bolus injection at 3 mg·kg-1. Mice were anesthetized using isoflurane and 50 µL of blood was collected at 0, 0.25, 0.5, 1, 2, and 4 hours post compound administration. Each mouse received two survival bleeds for total collected volume of 100 µL or <10% total animal blood volume in accordance with animal welfare regulations[81]. Terminal bleeds were collected at 6, 8, and 24 hours post compound

administration. Survival bleeds were drawn from the facial vein and terminal bleeds via cardiac puncture following CO2 asphyxiation[81]. Three mice were used per time point.

Blood samples were centrifuged (3,000 x g, 15 min) for plasma separation. 10 µL aliquots of plasma were extracted with two 500 µL equivalents of methanol containing 0.1% formic acid to ensure maximum recovery of compound from plasma. The supernatant was collected from precipitated protein pellet following centrifugation (3,000 x g, 5 min) and evaporated to dryness using a temperature-controlled Eppendorf Vacufuge at 30°C for 4 hours. The dry samples were reconstituted with 100 µL of methanol (1:10 original analyte dilution factor) spiked with 250 ng·mL-1 verapamil (Sigma-Aldrich) as an internal standard and subjected to LC-MS analysis on a Bruker Daltronics micrOTOF-Q II mass spectrometer coupled with an Agilent 1200 Infinity series HPLC with temperature controlled autosampler (24°C) and photodiode array detector. Standard solutions of compound ranging from 1000 ng·mL-1 to 7.8125 ng·mL-1 spiked into mouse control plasma was also analyzed to generate a calibration curve corrected for matrix effects. A linear regression generated from calibration samples was used to quantify

samples. The LOD of the LC-MS method was approximately 2 ng·mL-1. A 4.6 X 100 mm Kinetex® 2.6 µm EVO C18 100 Å column at a flow rate of 0.5 mL·min-1 was used in the analysis. The mobile phase consisted of water containing 0.1% formic acid as solvent A and acetonitrile with 0.1% formic acid as solvent B. The gradient conditions were maintained as follows: 90% A, 10% B to 100% B in 8 min; 100% held for 4 min as a washing step; 100% B back to 90% A in 2 min; 90% A, 10% B held for 3 min to reset and equilibrate the column.

Each analytical run was automatically calibrated using a secondary line injection of 10 µL sodium acetate external standard at 13 min. The injection volume of the analyte was 10 µL and MS was operated in positive mode with electrospray ionization at source. Mass spectra were monitored in a range of 50 to 1000 m/z. Data was processed using DataAnalysis 4.1 and QuantAnalysis (Bruker Daltronics). PK values were calculated using PKSolver[82].

RESULTS

Triazinoindol-benzimidazolone analog evaluation

In an attempt to build upon Sivendran et al, five additional compounds were purchased from Chembridge to explore substitutions of the benzimidazole moiety as well as a substitution of the R_1 position[1]. As Sivendran had already demonstrated that groups added at R_2 resulted in a dramatic loss of activity, we did not explore R_2 substitutions. Compound 7049574 is identical to 6904191 but with a longer linker on the phenyl group. The other four compounds were chosen to further probe the active site as well as substitute the benzimidazole moiety with one that would increase the polar surface area without sacrificing inhibition. An increased polar surface area is associated with improved oral bioavailability. The ClogP of the triazinoindol-benzimidazolones was often in conflict with Lipinski's rules or borderline. Our testing of the kinetic solubility of the compounds from Sivendran et al confirms this, suggesting they would likely have poor oral bioavailability[1].

None of the new compounds were amenable to cocrystallization or soaking. After solving the structures of known potent triazinoindol-benzimidazolones, it became clear that the benzimidazole moiety is essential for activity. The benzimidazole moiety mimics the deoxyriboside residue of the substrate and forms a strong pi-pi stacking interaction with TYR138. Assuming a maintenance of a similar mode of binding, the benzimidazole must be replaced with a residue also capable of pi-pi stacking with TYR138.

Compound 5225634 is lacking the benzimidazole entirely without a substitution to determine the role the triazinoindol plays in binding. We did not observe density in the active site, suggesting that the benzimidazolone group may play a more pivotal role and that substitutions of the triazinoindole group may instead be the more desirable substitution.

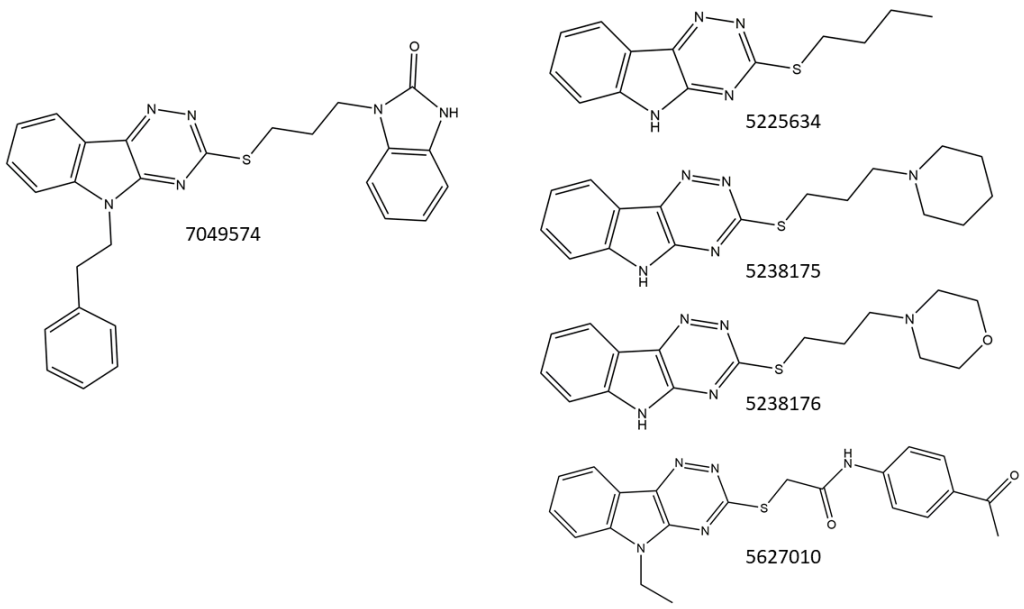

Figure 6: Triazinoindol-benzimidazole analogs

Kinetic solubility

rmlC compounds 6665037 and 7093044 were tested for kinetic solubility. As predicted based on calculated log P values of 4.12 for 6665037 and 5.18 for 7093044, the compounds exhibited very poor solubility. 7093044 was completely insoluble and 6665037 was only soluble to 2 µM. However, reported rmlD inhibitor 5104346 exhibited a considerably higher kinetic solubility, up to 98 µM.

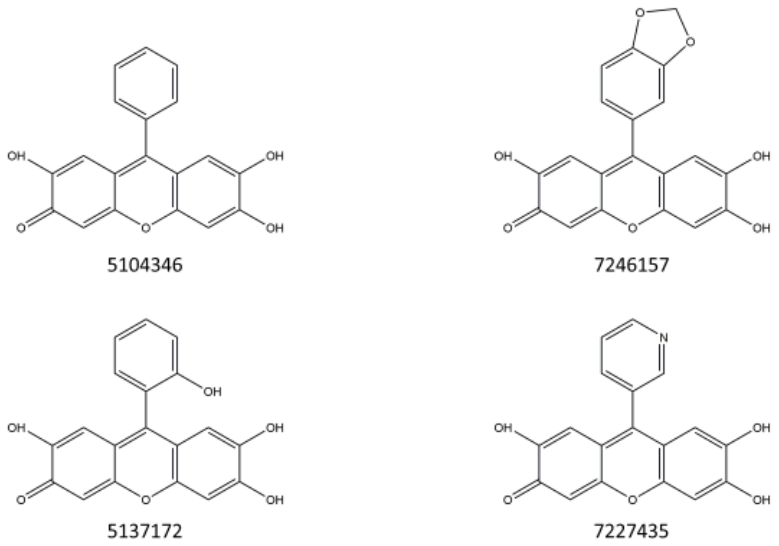

Figure 7: RmlD inhibitor compounds

Compounds from virtual screening reported in Wang[2] and our analogs chosen based on active site modeling. 5137172 and 5104346 from Wang have high enzymatic inhibition but poor whole cell activity.

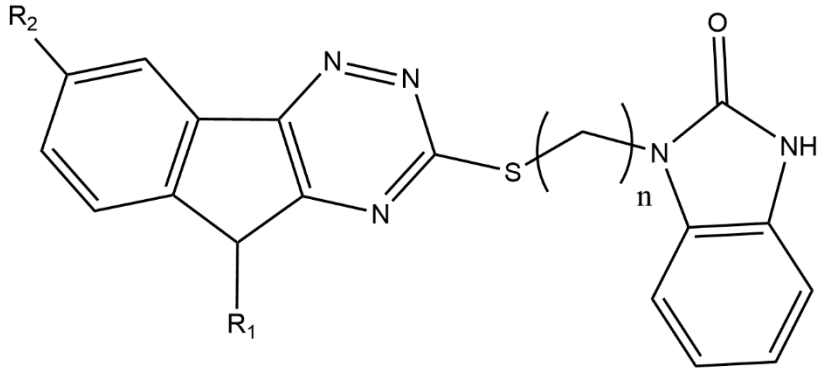

Compound ID	R1	R2	*n*	IC50 (µM)	MIC (µg/mL)
7077074	CH2=CH-CH2	H	3	0.12	13
6892686	CH3-CH2	H	3	0.2	19
6665037	CH3-	H	3	0.5	9
7093044	CH3-CH2-CH2	H	3	1.25	9
6904191	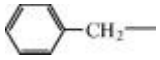	H	3	2.9	>50
6922675	H	H	3	3.3	ND
78531	CH2=CH-CH2	CH3	3	20	25

Figure 8: Triazinoindol-benzimidazolone scaffold and IC50's

Triazinoindol-benzimidazolone scaffold with associated R-groups and IC50 values alongside Mtb MIC values[1]

The core molecule picture above was tested with substitutions at various positions, denoted in the chart. IC50 values were calculated from enzyme assays and the MIC values were determined from testing on *M. tuberculosis* cells.

Plasma Protein Binding

Plasma protein binding results of two compounds thus far suggest this series, as is, has a very high percentage bound. Without further study, it is difficult to suggest whether the concentration of drug would be sufficient to kill *M. tuberculosis* in vivo. 6665037, with a methyl substitution at R1, displays a slightly lower plasma protein binding than 7093044 with its propyl substitution.

Compound	% bound	St. Dev.
6665037	97%	0.004
7093044	>99%	0.001

Table 1: Plasma protein binding results

Results were obtained for two of the triazinoindol-benzimidazolones. Both compounds show considerable plasma protein binding, which may affect the concentration of drug being high enough at the site of infection.

Crystal structures of triazinoindol-benzimidazolones

Multiple RmlC-inhibitor complex structures were solved to examine structural features and interactions of the inhibitors with the active site. Crystal structures were obtained of 7077074, 6892686, 6665037, 6922675, and 7093044. Cocrystallization proved sufficient to visualize bound inhibitors in the active site.

Upon observing the completed structures it became apparent why 6904191, with its methylphenyl substitution was R1, was not amenable to a crystal structure despite having an IC50 only slightly more than the others. 6904191 only shows weak electron density. The symmetry mate's His19 R-group does not allow for such a large hydrophobic residue to bind well in a crystal structure. This would not occur in solution, hence why a relatively low IC50 of 2.9 µM is observed.

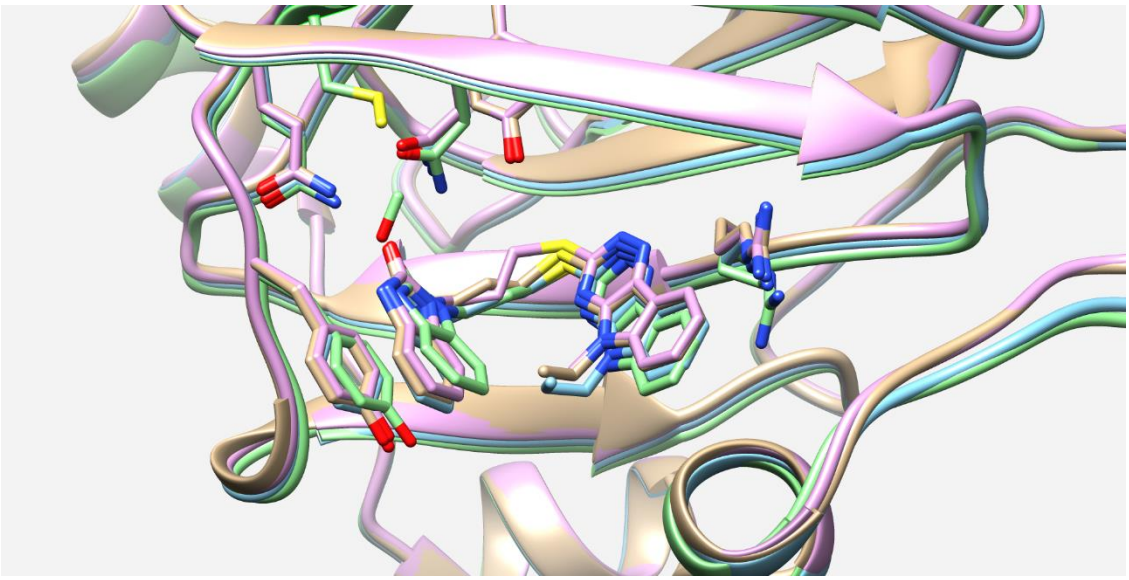

Figure 9: 5 RmlC inhibitor structures overlayed

Only 6922675 (light green) shows a notable but minor deviation. The lack of a group at R1 disallows a hydrophobic interaction between the benzene ring of the benzimidazole moiety and small carbon chains found in other inhibitors.

Tyr138 and Arg59 are notably disturbed, with the guanidino group of Arg59 shifted 1.7 Å and the hydroxybenzene of Tyr138 shifted 1.0 Å. This shift is very unfavorable, resulting in an IC50 ranging from 3 to 27 times higher than other inhibitors solved.

DISCUSSION

In 2010 Sivendran et al published a report on the triazinoindol-benzimidazolone class of compounds discovered via high throughput screening[1]. The study included multiple analogs picked from the library and evaluated enzymatically and docked. To date, no structures of rmlC with any triazinoindol-benzimidazolone, or any inhibitor, have been published. Presenting an opportunity for further evaluation with experimental data, the structures of multiple triazinoindol-benzimidazolones were solved in complex with Mtb rmlC. The structures were also compared to the published docking models. An explanation for why specific R-groups provided greater enzymatic inhibition was forthcoming in our analysis.

Two docking models were presented in Sivendran, with one significantly more in agreement with our structure. However, using the solved pathway product structure as the docking model resulted a model with the triazinoindol-benzimidazolone positioned akin to dTDP-rhamnose in the solved structure. The benzimidazolone moiety still forms the pi-pi stacking interaction with Tyr138. However, the

rest of the compound is positioned deep within the active site.

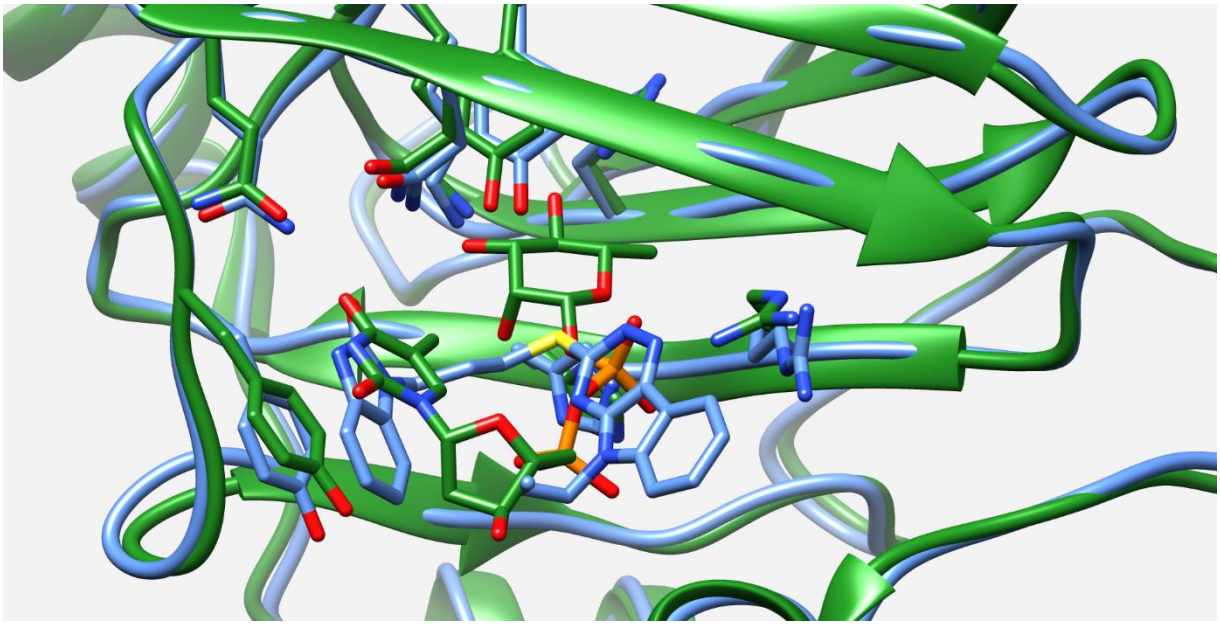

Figure 10: 7093044 structure

Overlay of 7093044 structure (blue) with dTDP-rhamnose structure (green). The rhamnose moiety of dTDP-rhamnose resides deep within the active site in contact with the catalytic residues Tyr132, Lys72, and His62. Active site residues are largely unchanged, save for a 2.5 Å movement of Arg59 towards the product phosphodiester linkage.

As shown in the above figure, the triazinoindol-benzimidazoles make no contact with any of the catalytic residues. This may explain why the compound series is so potent despite making few strong bonds. By sitting at the surface of the active site rather than inside the active site, the substrate and the triazinoindol-benzimidazolones compete for few interactions. The triazinoindol-

benzimidazolones effectively serve as a lid over the active site, preventing substrate access.

Only one substitution at R2 was assayed. In Sivendran, it was hypothesized based on the docking model that the addition of a methyl group at the R2 position will cause steric clash with His119 and Phe121. Upon solving the crystal structure, it became apparent this was not the case. The addition of a methyl at R2 would put it within close proximity to the guanidino group of Arg59. This decrease in solvation of Arg59 is energetically unfavorable and also introduces an interaction between the hydrophobic methyl group and the hydrophilic guanidino group. In addition, the methyl group would push Arg59 towards Val57, sandwiching Arg59 between two hydrophobic moieties.

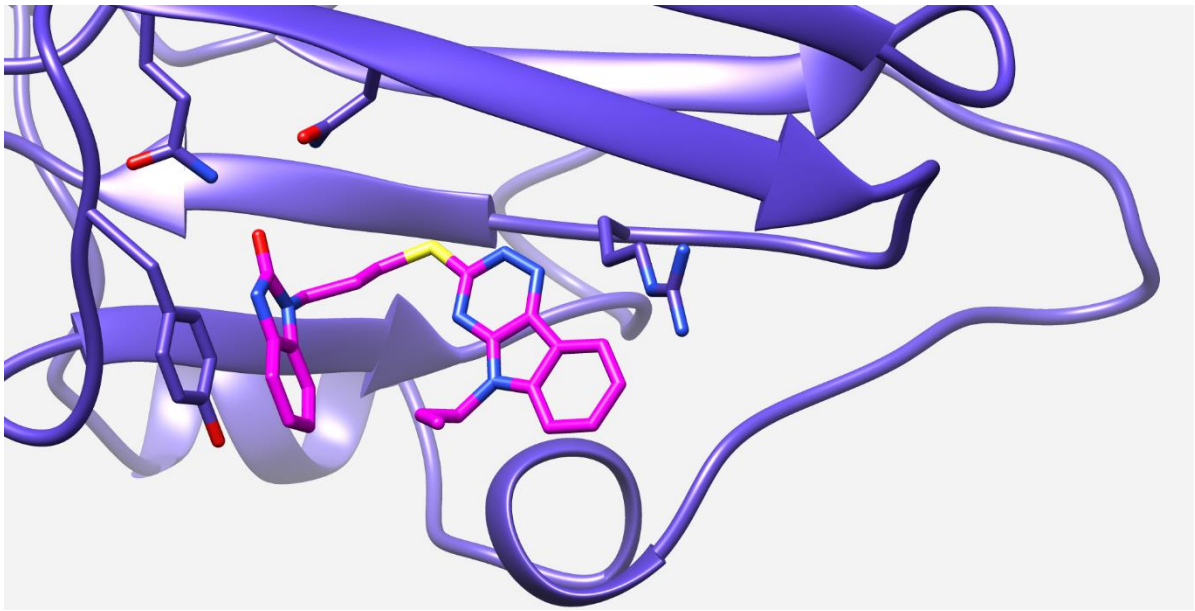

Figure 11: 7093044 structure showing effects of R2 substitution

Structure of 3044, with emphasis on Arg59 (right), suggesting a major perturbation would result from a methyl substitution at R2

The substitutions at R1 play a significant role in binding. The length and type of carbon chain affects the hydrophobic interaction the triazinoindol-benzimidazolones have with themselves. Commonly referred to as a hydrophobic interaction, it could be argued that hydrophobic exclusion is a more appropriate term. This refers to the observed tendency of nonpolar substances to aggregate in an aqueous solution and exclude water molecules[83].

Research into hydrophobic interactions have a well-studied but storied history[84]. The hydrophobic interaction is responsible for the low solubility of hydrophobic molecules in water. This has a central role both micelle formation and the structure of proteins[85, 86]. The strong tendency of hydrophobic molecules to aggregate in a polar solution was such that there was once suspected to be a “hydrophobic bond” associated with it[85, 87]. It is now recognized that the hydrophobic interaction involves the configurational rearrangement of water molecules as two hydrophobic species come together in solution[88-91]. The hydrophobic interaction has an effect over a much wider area than a typical covalent bond. Measurements show that the hydrophobic interaction has roughly the same range as the van der Waals-dispersion force but is about an order of magnitude stronger. The strength of the hydrophobic interaction decays exponentially over the range of 0–10 nm[92].

The most potent of the triazinoindol-benzimidazolones are ones with no substitutions at R2 and small, hydrophobic carbon chains at R2. The hydrophobic effect and the shape of the hydrophobic regions of the inhibitors is largely responsible for the potency, with only two

hydrogen bonding interactions between the O01 oxygen of 7093044 and the ND2 and NE2 nitrogens of Asn49 and Gln47, respectively.

Noting the essentiality of the pi-pi stacking between the benzimidazolone group and Tyr138, it is reasonable to suggest a simple point mutation would render these compounds ineffective. However, Tyr138 also forms this same interaction with the substrate's thymidine group. While a mutation to phenylalanine would still allow the substrate to position itself, the inhibitors would also still have a benzene ring to interact with.

The lack of observed toxicity with any compounds in the series suggest the triazinoindol-benzimidazolones may a starting point as a scaffold, with modifications in the triazinoindol group, or possibly a different group altogether, to increase kinetic solubility[93]. As of now, it appears to largely serve as a placeholder, only making interactions with Arg59.

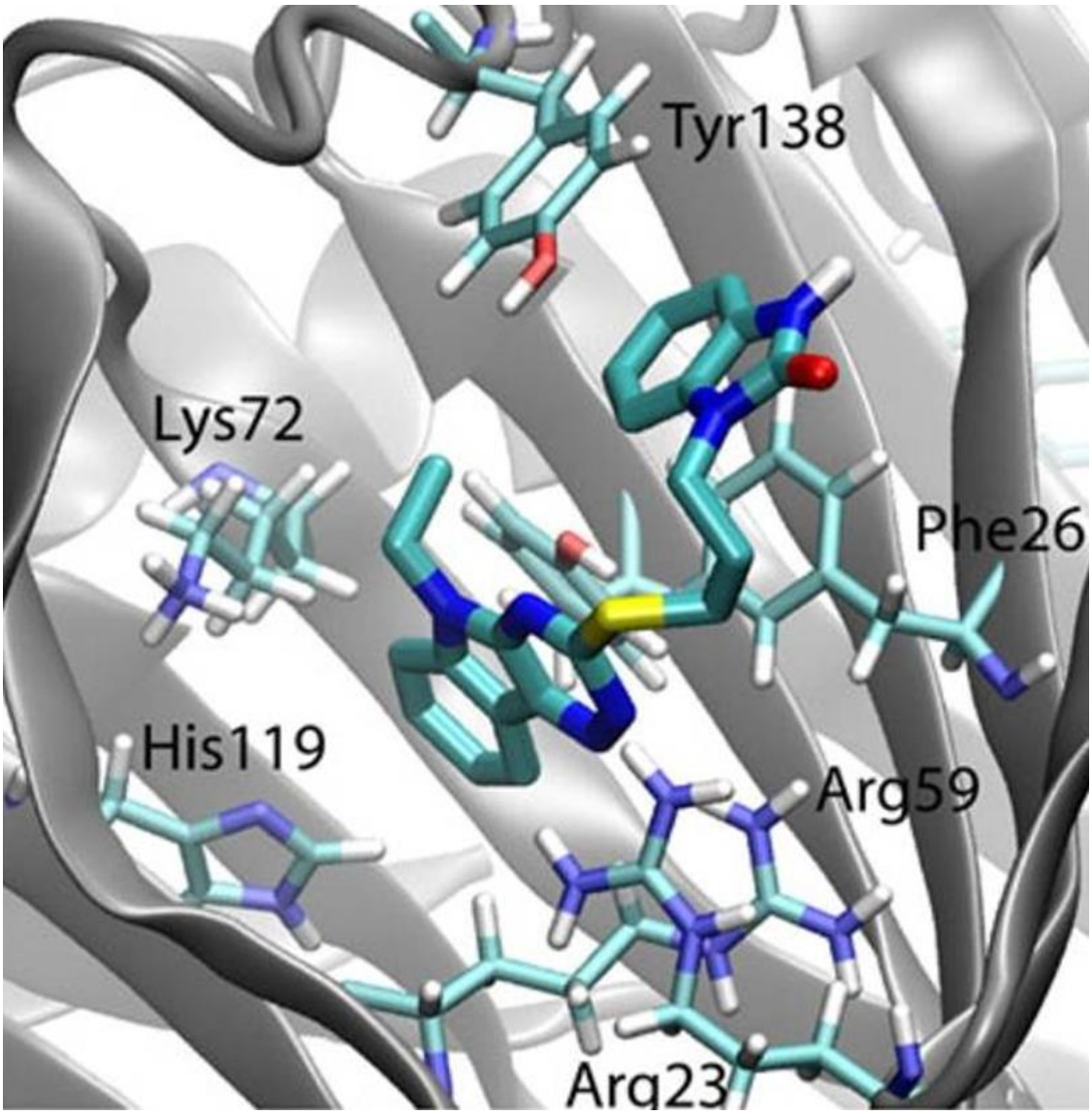

Figure 12: Docking structure of RmlC-6892686[1]

The benzimidazolone pi-pi stacking with Tyr138 is in agreement with our crystal structures, while the triazinoindol group is found at the mouth of the active site rather than in contact with active site catalytic residues deeper within

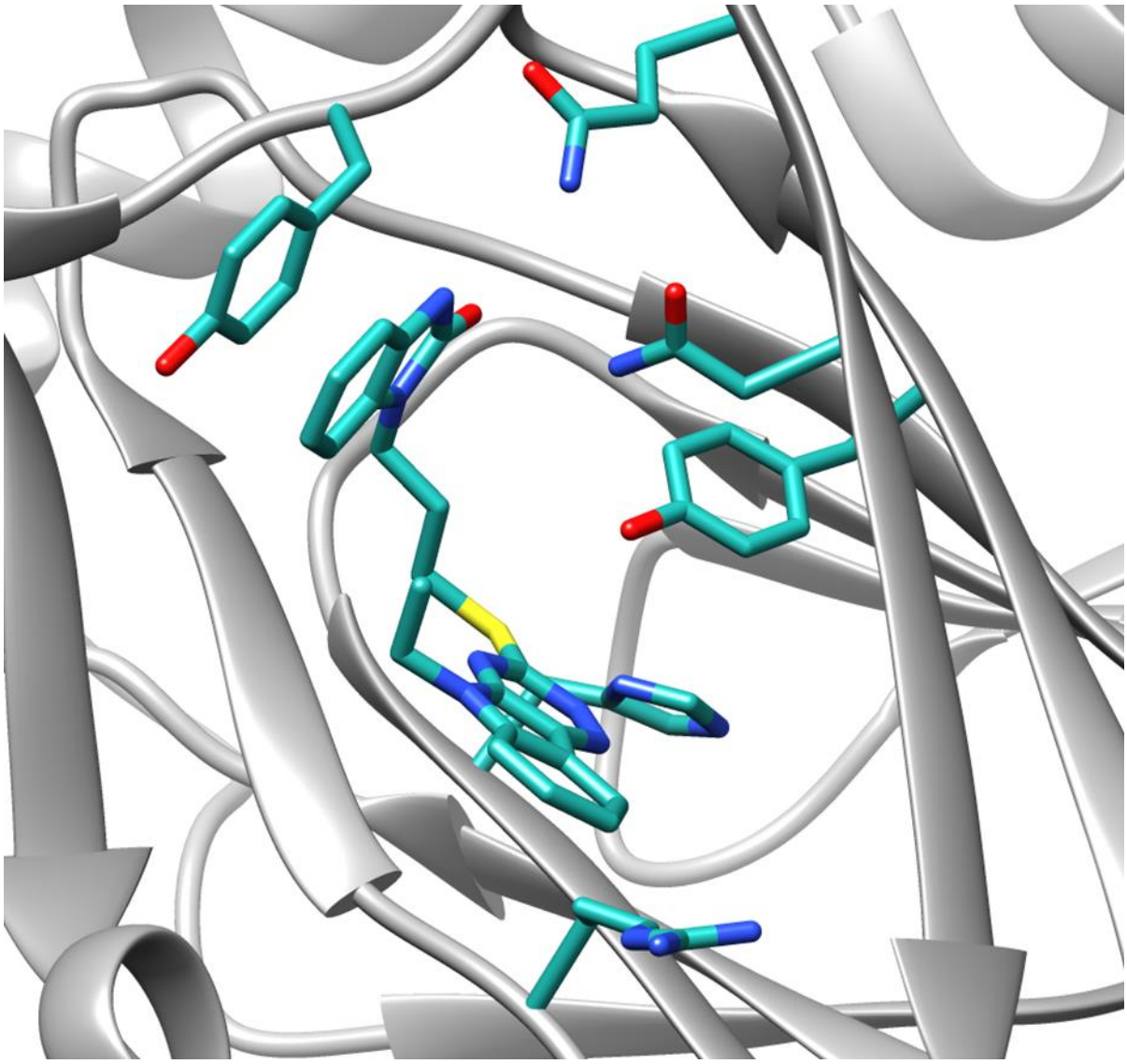

Figure 13: RmlC-6892686 structure

The pi-pi stacking interaction between Tyr138 is consistent with the docking model. However, the benzimidazolone orientation is reversed and the triazinoindol is on the periphery of the active site as opposed to deep within it

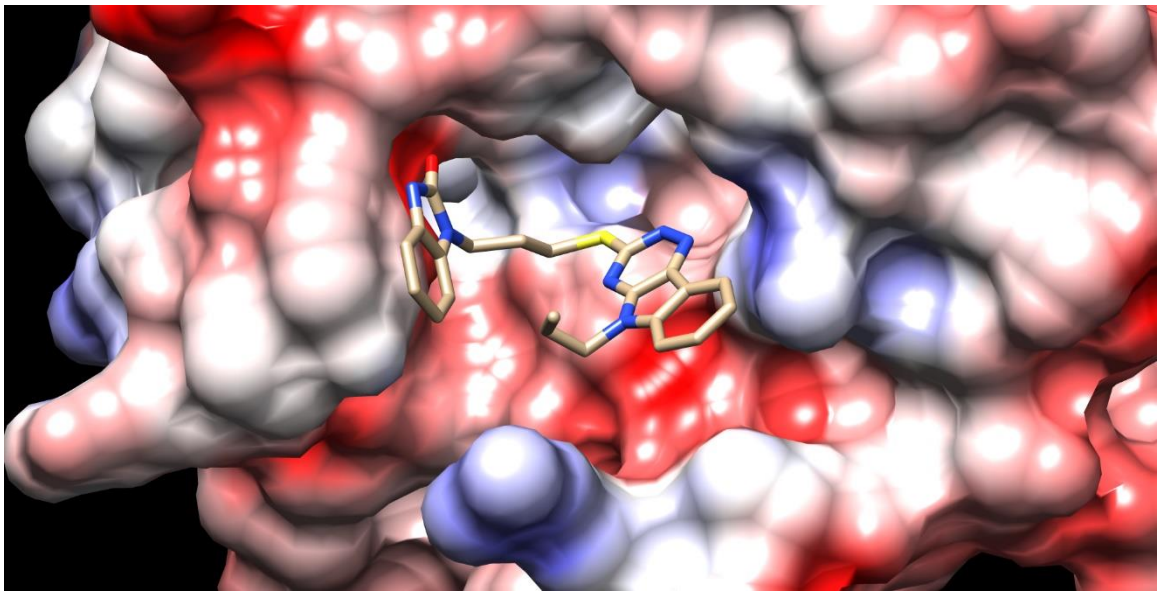

Figure 14: RmlC-7093044 electrostatic map

Electrostatic potential surface map of rmlC with 7093044 bound. There are considerable empty regions available for modifications to the compound series.

In particular, the addition of a hydroxyl group to the end of the propyl moiety of 7093044 would likely hydrogen bond with the Arg170's positively charged guanidino group. Currently, the propyl group makes no bonds and contributes to the high ClogP. The ClogP decreases dramatically with the change, from 5.18 to 3.60.

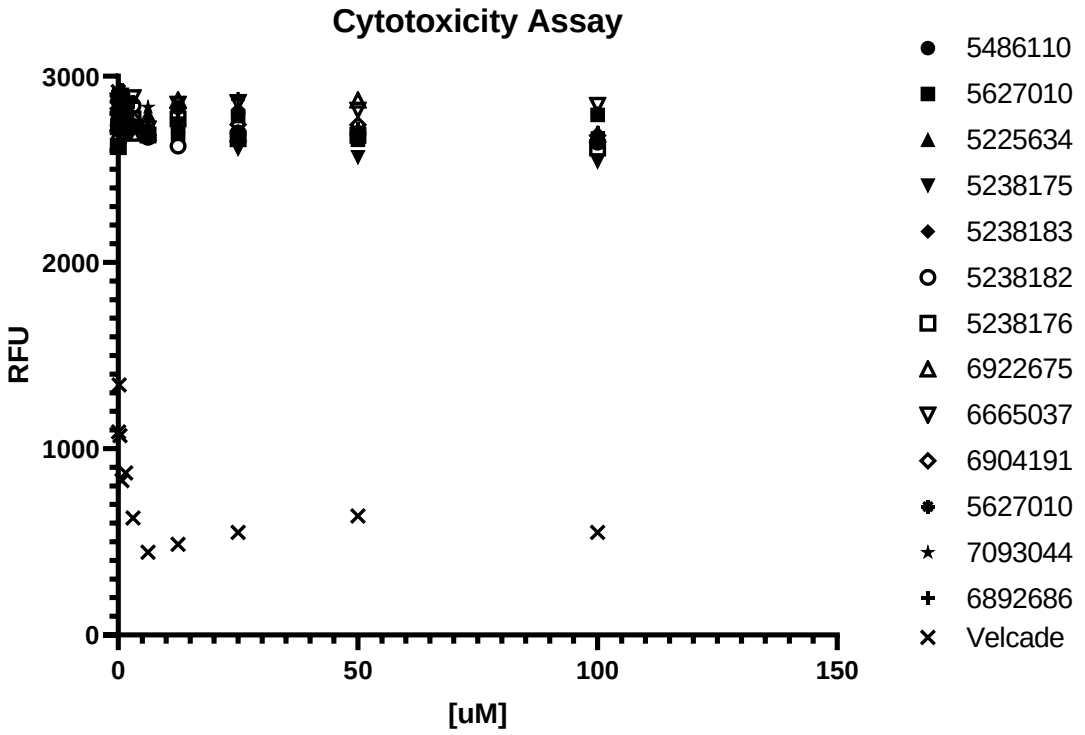

Figure 15: Cytotoxicity data of inhibitors

No compounds show any significant toxicity up to 100 µM. Velcade was used as a negative control.

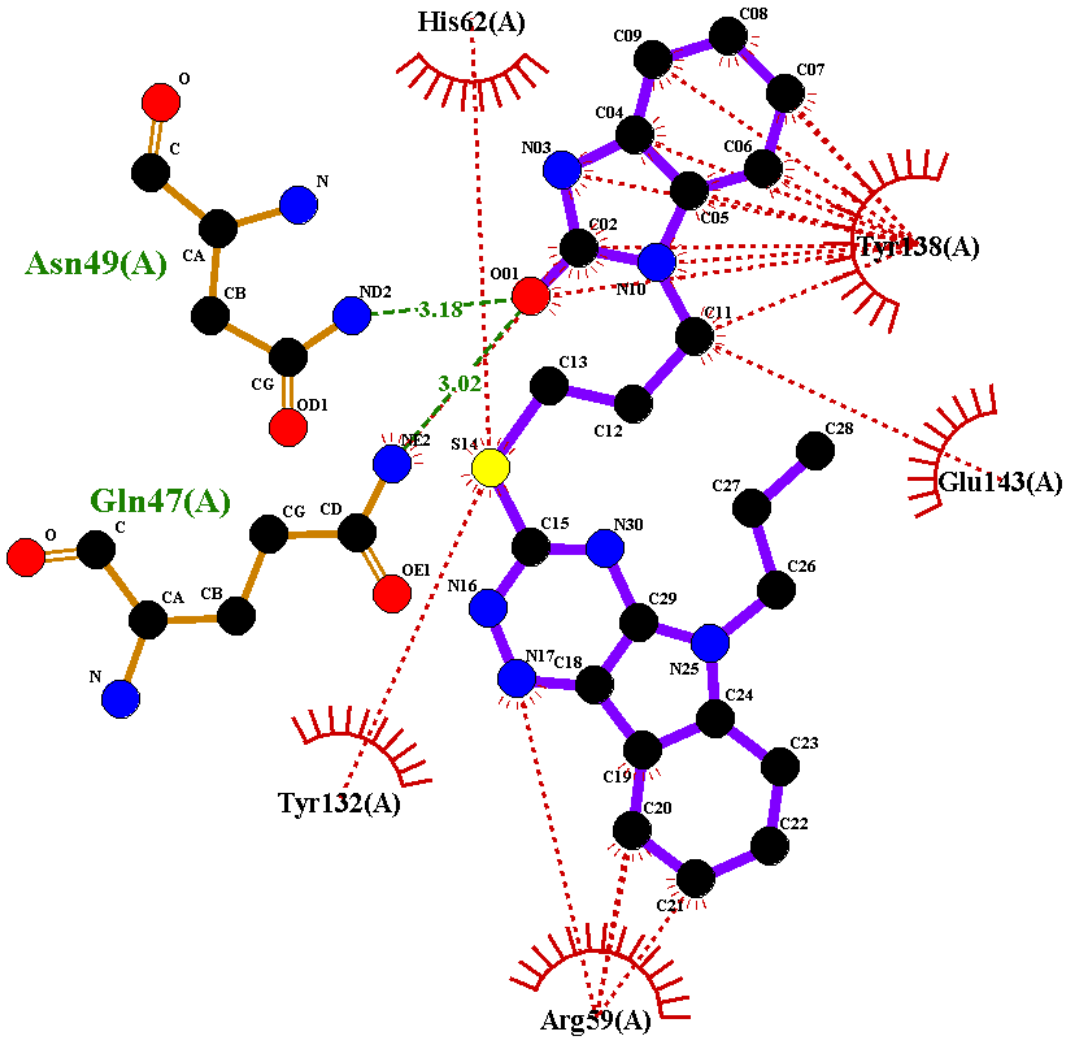

Figure 16: Ligplot diagram of 7093044 interactions

Two hydrogen bonding interactions between the O01 oxygen of 7093044 and the ND2 and NE2 nitrogens of Asn49 and Gln47, respectively.

The predominant hydrophobic interaction is between Tyr138 and the benzimidazolone moiety of 7093044.

CHAPTER III

STRUCTURAL AND FUNCTIONAL INSIGHTS INTO INHIBITION OF UDP-N-ACETYLGLUCOSAMINE ENOLPYRUVYL TRANSFERASE IN PSEUDOMONAS AERUGINOSA

OVERVIEW

Pseudomonas aeruginosa is the causative agent for an estimated 51,000 infections in the United States each year, including 400 deaths. The bacterium is inherently resistant to most clinical antibiotics, with some exceptions including fluoroquinolones and specific β-lactams. To date, there has been only a single PDB deposition of *P. aeruginosa* MurA with no associated publication or analysis. We present a detailed analysis of *P. aeruginosa* MurA with various inhibitors, substrate, and product. To produce this analysis, we soaked or co-crystallized MurA with these compounds to capture them in the active site. While the MurA enzymes exhibit very high homology across species, slight variations between published structures and *P. aeruginosa* are observed. The inhibitor structures successfully obtained were of covalent modifiers, including fosfomycin and terreic acid.

We also evaluate published enzymatic inhibitors for their whole cell activity. The only recently published enzymatic inhibitor that exhibited whole cell activity was carbidopa, a dopamine decarboxylase inhibitor administered to people with Parkinson's disease in order to inhibit peripheral metabolism of levodopa. Additional dopamine decarboxylase inhibitors, benserazide difluromethyldopa, and α-methyldopa, are available and may provide a starting point for designing a MurA inhibitor capable of killing *P. aeruginosa*.

INTRODUCTION

The antibiotic fosfomycin is able to treat non-resistant strains of *P. aeruginosa*, however, increasing pressure from resistance mechanisms including FosA, multi-drug efflux pumps, and C115 mutations have accelerated the need to have alternative treatments. Given the covalent nature of fosfomycin, a mutation in C115 results in a near complete resistance to the drug’s effects. While certain β-lactams remain efficacious against more standard strains, the increasing spread of resistance genes in *P. aeruginosa* such as the notorious NDM-1 metallo β-lactamase

suggest that reliance on β-lactams should be a resort of decreasing reliance as the resistance rates outpace the creation of newer and more effective drugs[94-96].

The inhibitor class commonly associated with MurA is one of covalent modification. Many attempts at creating analogs of fosfomycin have been attempted but have not been effective enough for continued consideration[97]. Issues range from lack of whole cell efficacy to toxicity from nonspecific cysteine modification. Fosfomycin is remarkable for its ability to only modify the active site cysteine in MurA, without peripheral and nonspecific side effects[98]. It is absorbed and excreted in the urine unchanged[99]. However, the reliance on covalent modification has resulted in some strains of *P. aeruginosa* having a mutation from cysteine to aspartate, resulting in fosfomycin bactericidal activity being abolished[100]. Indeed, the *Mycobacterium tuberculosis* MurA has long been known to be immune to the effects of fosfomycin and this comes from the wild type MurA containing aspartate instead of cysteine[101].

This reliance on covalent modification begs a question. Why are there no approved drugs that utilize a different mechanism of action? It is worth noting that the

purified enzyme, depending on the bacterial species from which it is derived, almost always contains the substrate UDP N-acetylglucosamine or the MurB product, UDP MurNac, bound to the active site[102]. Attempts to remove it with repeated washings or high ionic strength conditions proved futile. The large substrate (607.35 g·mol−1) contains many interactions with the active site and the mechanism by which the enzyme operates necessitates the binding of UDP N-acetylglucosamine first[103]. The tight binding could be considered to be a defining reason why inhibition by a different mode of action has had limited success.

If efforts are steered away from covalent modification and competitive inhibition via the region of the active containing UDP N-acetylglucosamine, that would present the region where phosphoenolpyruvate (PEP) reacts with UDP-N-acetylglucosamine as a potential target. This region has a degree of solvent exposure and could theoretically provide a means to be a site of inhibition against phosphoenolpyruvate.

MurA presents itself as an excellent candidate for antibiotic design, as it is an essential, highly conserved enzyme across Gram-negative and Gram-positive bacteria and there is no known human counterpart. While certainly there

exist very successful cases of targeting enzymes found in both humans and bacteria, the task of designing a new drug is theoretically less burdensome without concern for cross reactivity with the human homolog. For instance, the macrolides are a common antibiotic used to treat bacterial infections. They have long been known to target the bacterial ribosome. However, certain macrolides such as kanamycin have been supplanted by alternatives because of well-documented side effects, including ototoxicity[104, 105]. Even the to this day commonly prescribed azithromycin has a documented history of causing permanent hearing loss[106]. It has been shown that macrolides have varying degrees of inhibition against the human ribosome[107]. This cross reactivity is why certain macrolides have either never made it to FDA approval or have been largely shelved, although examples such as azithromycin have been weighed and found that the risk potential is exceeded by its therapeutic value.

By creating a comprehensive structure-based analysis of *P. aeruginosa* MurA, we elucidate both the similarities and differences among these bacterial enzymes. Furthermore, we offer a structural explanation for the differential potencies of fosfomycin in P. aeruginosa

versus known MurA-fosfomycin structures solved in other bacteria. The P. aeruginosa MurA is, to date, lacking any published structural analysis and this body of work addresses this missing component in the MurA literature.

MATERIALS AND METHODS

Cloning, expression, and purification

Wild-type MurA was amplified from *P. aeruginosa* PAO1 genomic DNA using Phusion polymerase from New England Biolabs and inserted into the NdeI and HindIII sites in pET28b. Forward and reverse primers were TTTTTTCATATG GATAAACTGATTATTACCGGCGGTAACC and TTTTTTAAGCTTCTAGCCCGGTACGCG, respectively. These resulted in an N-terminal hexahistine tag. Sequences were confirmed by Eton Bioscience. Plasmids were transformed into the Invitrogen *E. coli* BL21 (DE3) strain. To produce the protein, the bacterial cultures were grown at 37°C at 180 rpm in LB medium until an OD600 of 1.0 was reached. Following cooling down to 20°C for 60 minutes, the cultures were induced with 1.0 mM isopropyl-β-D-thiogalactoside. The cells were incubated overnight at

20°C, harvested and resuspended in lysis buffer (10% glycerol, 100 mM NaCl, 25 mM $(NH_4)_2SO_4$, 10 mM imidazole, 20mM HEPES pH 7.4, and 0.5 mM TCEP). Cells were disrupted via French Press at 20,000 PSI and the insoluble cellular material was removed by centrifugation at 13,000 rcf for 1 hour. MurA purified using Ni-NTA affinity chromatography in a gravity column through multiple volumes of wash lysis buffer until eluent samples no longer produced a visible color change with Bradford protein quantification reagent, indicating washing was complete. Proteins were eluted with elution buffer (5% glycerol, 50 mM NaCl, 25 mM $(NH_4)_2SO_4$, 200mM imidazole, 10mM HEPES pH 7.4, and 0.5 mM TCEP) until eluent samples no longer produced a visible color change with Bradford protein quantification reagent, indicating elution was complete. Samples were then concentrated using Millipore Amicon Ultra-15 centrifugal filter units and injected onto a GE S200 size exclusion chromatography column. Peaks corresponding to the target protein were collected and concentrated to 12 mg/mL. Individual aliquots of purified protein were stored at -80°C until needed.

Size exclusion chromatography

The molecular weight of MurA in solution was determined by size-exclusion chromatography using a Superdex 200 GE Healthcare 16/60 column. The column was calibrated with aprotinin (6.5 kDa), carbonic anhydrase (29 kDa), conalbumin (75 kDa), catalase (232 kDa), and thyroglobulin (669 kDa). The separation was carried out at 4°C at a flow rate of 1.0 mL/min. The calibration curve of Kav versus log molecular weight was prepared using the equation Kav= (Ve-Vo/)/(Vt-Vo,), where Ve = elution volume for the protein, Vo = column void volume, and Vt = total bed volume. Size exclusion chromatography indicates MurA is a protein dimer.

Crystallization

MurA was screened against crystallization sparse matrix screens Wizard, Index, Crystal Screen, and PEG/ION. Two forms of the protein, substrate-bound and product, were screened in a sitting drop vapor diffusion method at a ratio of 1:1 µL against 50 µL mother liquor. A suitable

condition for each was found after 48 hours. The substrate-bound condition is 12% MPD, 16% PEG 2000, and 10% Tacsimate pH 5.4. The product-bound condition is 24% PEG 2000 and 10% Tacsimate pH 5.8. Following initial hits, hanging drops were set up at a ratio of 3:3 µL and equilibrated against 0.5 ml of mother liquor to produce larger crystals. Crystals were transferred to a stabilization solution containing 30% glycerol in mother liquor and allowed to equilibrate for 10 minutes. Crystals were flash frozen in liquid nitrogen. Data Collection and Processing. X-ray diffraction data was collected on beamlines 19ID and 23ID at The Advanced Photon Source, Argonne National Laboratory, Argonne, IL. Data sets were reduced using HKL2000. Data was collected at a temperature of 120 K.

Sequence Alignment

An alignment of 10 amino acid sequences from deposited MurA structures in the Protein Data bank was performed using Jalview for visualization and Clustal for aligning. Sequence identity was also highlighted to show the high degree of conservation among MurA enzymes among

taxonomic classifications as high as phylum. The active site cysteine is boxed in red to show that it is conserved across phyla.

RESULTS

Whole cell inhibition

6 compounds were evaluated for their ability to inhibit or kill Pseudomonas aeruginosa strain PAO1. Only carbidopa showed any significant decrease in viability. *P. aeruginosa* is known to have multiple drug efflux pumps, giving it a wide resistance to small molecule inhibitors. These results are not entirely unexpected and reinforce the difficulty in developing inhibitors that are active against both the enzyme and the cell itself.

As we were unable to obtain a structure with carbidopa bound despite some enzymatic inhibition, we cannot rule out off target activity. Carbidopa was designed as a treatment for Parkinson's disease and not intended to treat bacterial infections. However, modifications to carbidopa as a lead molecule towards treating Pseudomonas may be feasible.

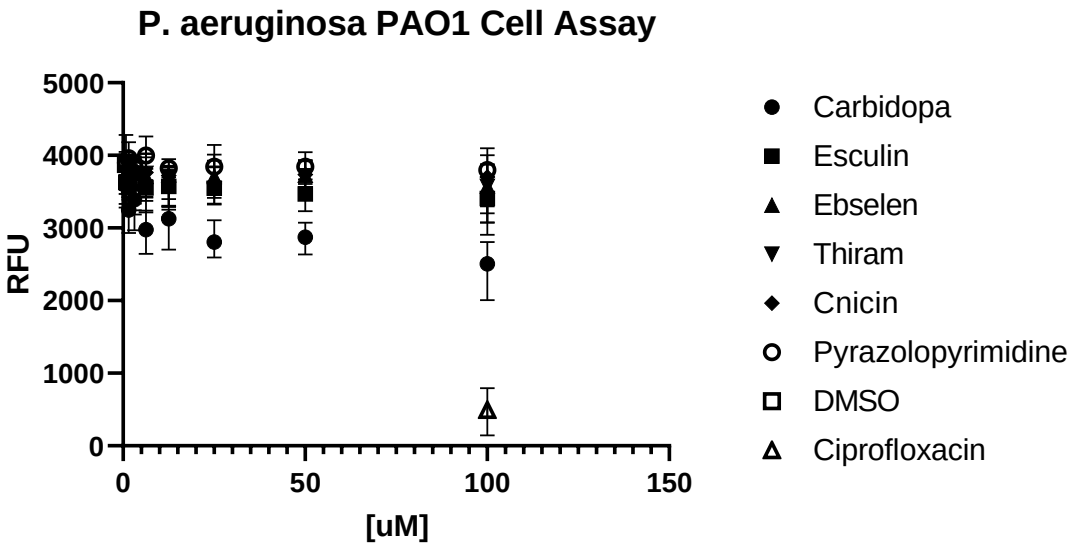

Figure 17: PAO1 whole cell assay

Effects of MurA enzymatic inhibitors against PAO1 *Pseudomonas auruginosa*. 100µM ciprofloxacin was used as a negative control and DMSO was used as a positive control

Crystallization and Structures

MurA proved amenable to crystallization, cocrystallization, and soaking. All crystals diffracted to ~2 Å or better, with low mosaicity.

Structures were solved of MurA with the co-purified substrate UDP-NAG, product UDP-NAG-EP, UDP-NAG and fosfomycin, UDP-NAG and terreic acid, and UDP-NAG-EP and fosfomycin.

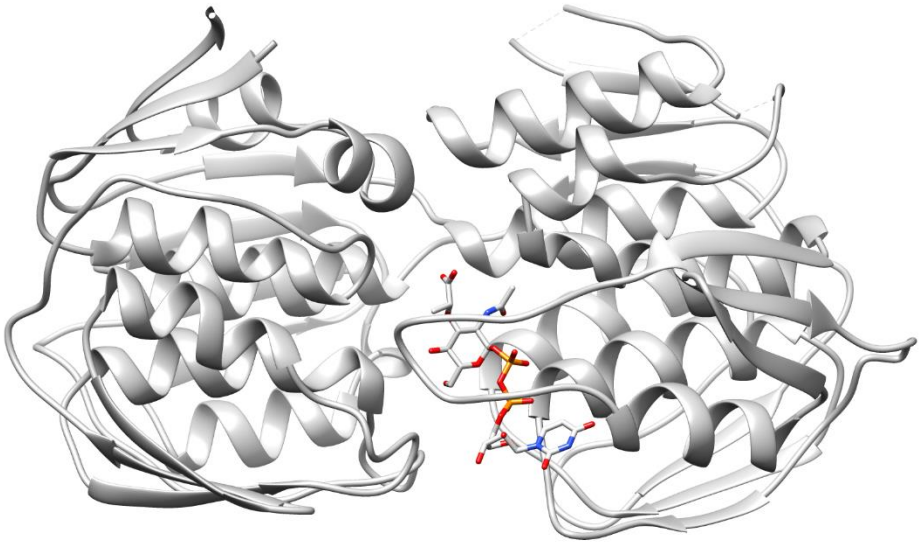

Figure 18: MurA-product structure

Structure of product UDP-NAG-EP within the active site of MurA. Note the active site lid in the foreground in front of UDP-NAG-EP. This loop opens and closes to allow substrate entry and product exit

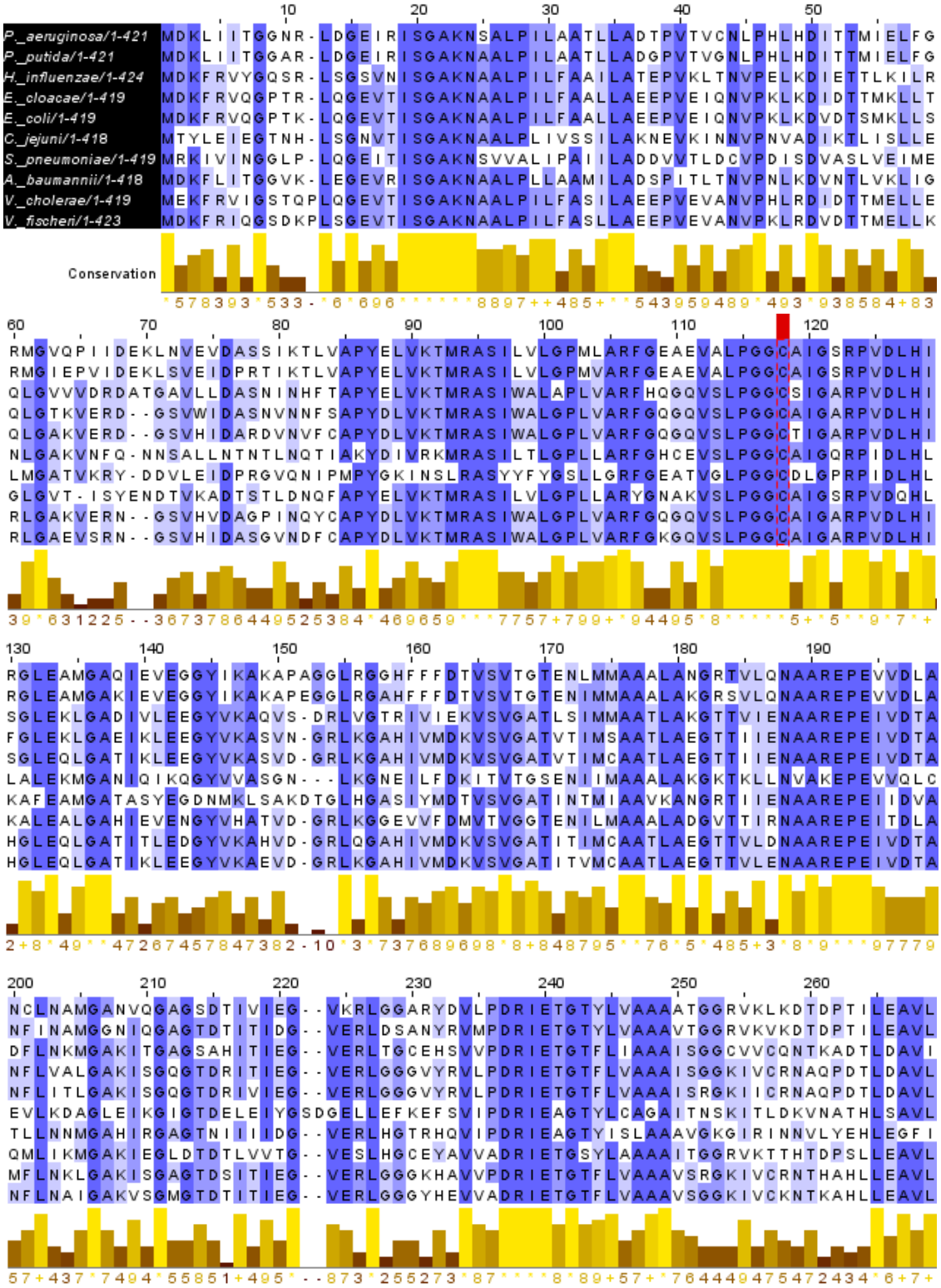

Figure 19 Sequence alignment of MurA from the PDB

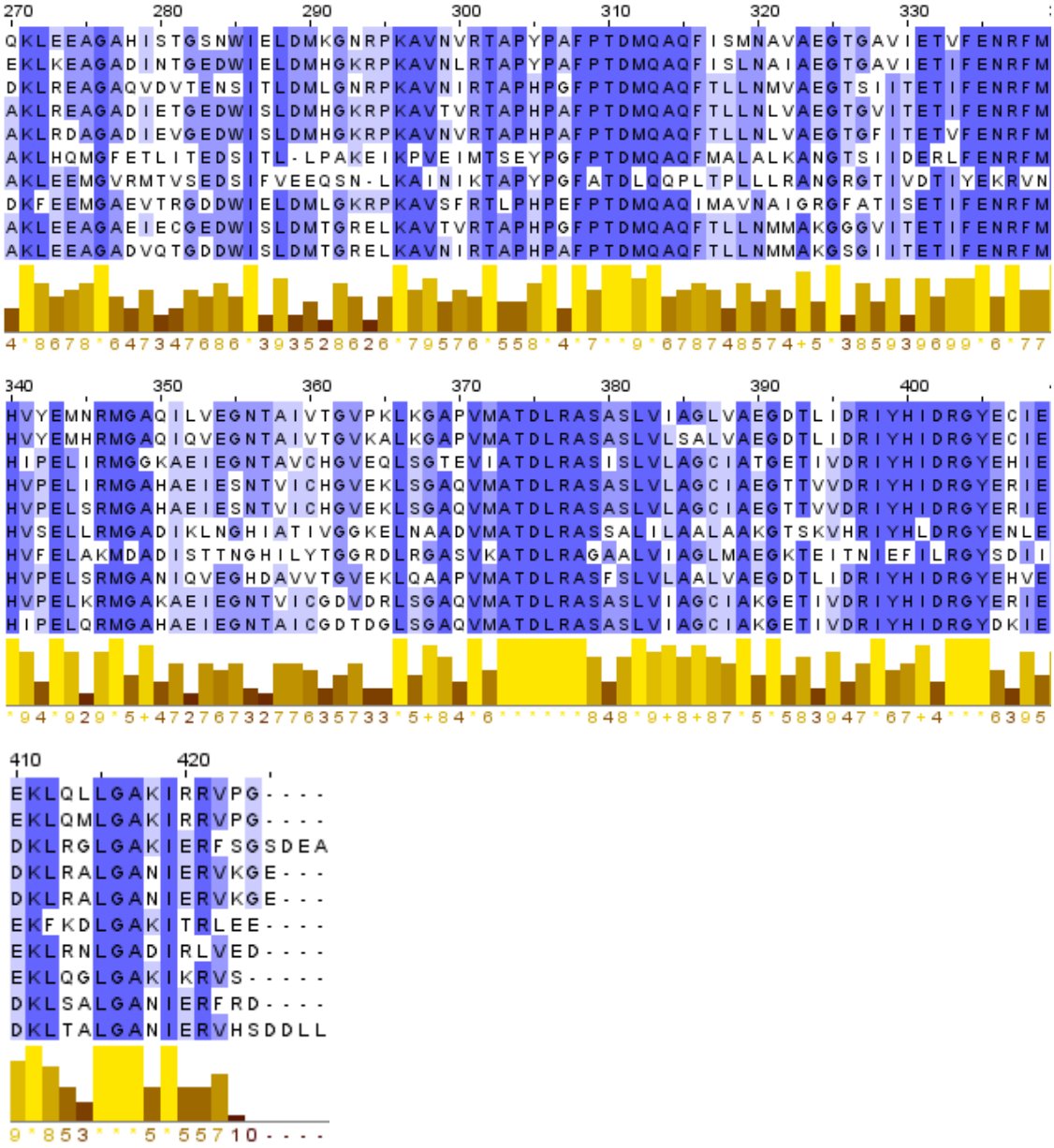

(continued) Figure 19: Sequence alignment of MurA from the PDB

Alignment of ten MurA amino acid sequences from structures deposited in the Protein Data Bank. Active site cysteine boxed in red. Despite members representing different phyla, the high degree of conservation showcases the ancient nature of peptidoglycan biosynthesis in bacteria.

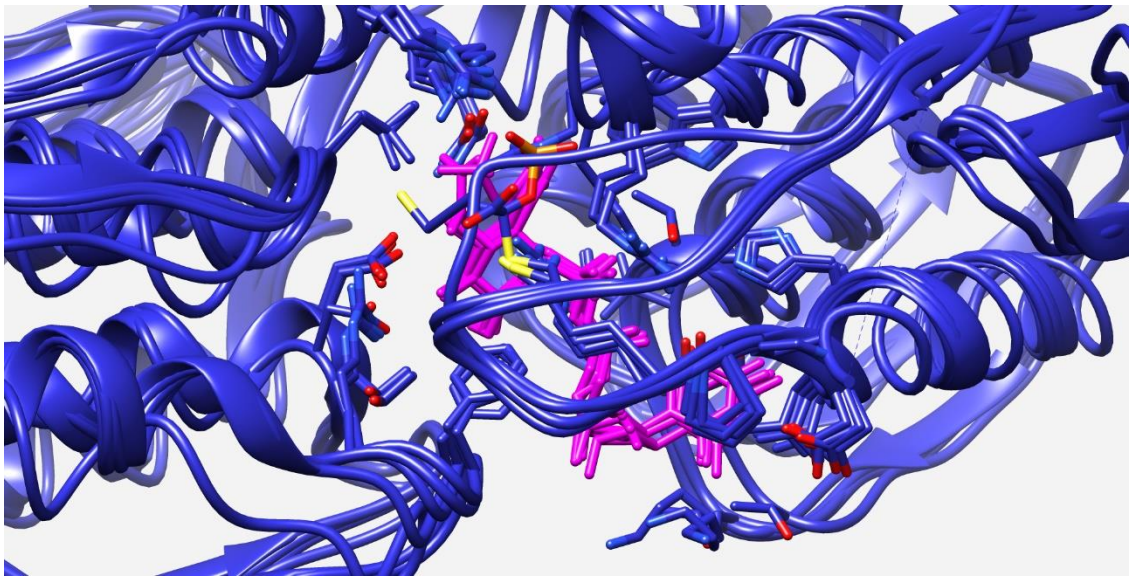

Figure 20: Overlay of pathogenic MurA structures

Overlay of 5 MurA structures from pathogenic species with the substrate UDP-NAG bound. The active site residues bonding with UDP-NAG are highly conserved, with the catalytic residues conserved entirely. The active site lid containing the active site cysteine is pictured in the foreground, with one example covalently bound to fosfomycin.

DISCUSSION

MurA has been a drug target for decades. However, no development of antibiotics has led to a treatment regimen save for the original and lone fosfomycin. Given the extensive and successful research into the downstream peptidoglycan biosynthetic enzymes, it is surprising that fosfomycin remains the sole source of antibiotics for the Mur pathway with no analogs. Dozens of antibiotics exist for targeting the transpeptidases and advancements continue to be made. However, β-lactamases have evolved and their genes spread among pathogenic species to the point that expecting them to continue to comprise over half of prescribed antibiotics presents a risk. The discovery of NDM-1 and tracking its spread among species elicited a panic throughout the medical and scientific professions, with concerns that if it became widely distributed it could have a major impact on treating infections with β-lactams often being the first prescribed antibiotic.

MurA presents itself as an excellent candidate for antibiotic design, as it is an essential, highly conserved enzyme across Gram-negative and Gram-positive bacteria and

there is no known human counterpart. While certainly there exist very successful cases of targeting enzymes found in both humans and bacteria, the task of designing a new drug is theoretically less burdensome if a balance between minimal human interference versus maximal bacterial interference need not be considered.

The *P. aeruginosa* MurA structure is highly similar in its overall fold to other MurA structures. This is expected given both the ubiquitous (in bacteria) and essential nature of MurA, lending to the high sequence conservation. Sequence similarity is often greater than 70%. As with other MurA structures, it exhibits the standard two globular domains connected by a double stranded linker. A loop containing C115 and other active site residues closes over the substrate UDP-GlcNAc upon binding. The domains are comprised of three parallel helices surrounded by three additional helices and three beta sheets.

Of the six compounds tested against cells, only carbidopa showed any efficacy and even then, only at concentration approaching 100 µM. Other compounds have been published that have greater potency, such as the

tulipalins, but with the critical problem of off target activity, leading to cytotoxicity.

One structure to note is the fosfomycin-product structure of MurA. This was unexpected because it was predicted that fosfomycin would not covalently bind to C115 if the product was bound. Indeed, no other MurA-fosfomycin-product structures have been published. While there are no notable structural differences between the fosfomycin-product and fosfomycin-substrate structures, this new structure shows that fosfomycin activity is not limited to only the substrate-bound MurA. It would be interesting to test other MurA's from published structures in other species to attempt to produce a MurA-fosfomycin-product structure. It seems unlikely that *P. aeruginosa* would be the only MurA capable of this, given the high sequence similarity.

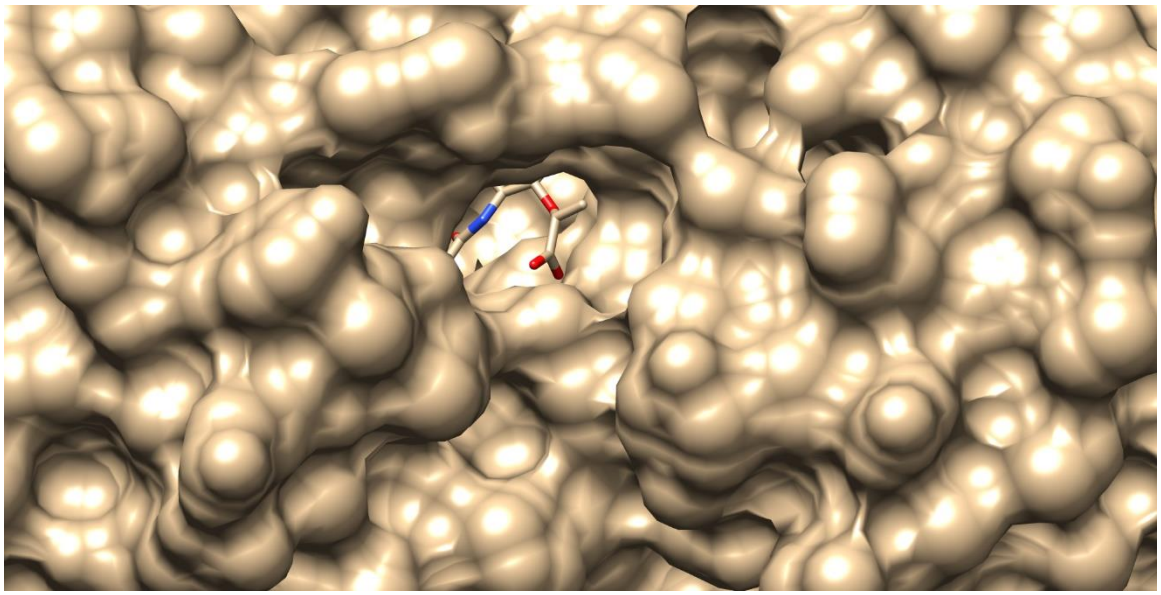

Figure 21: PEP hole in MurA-product structure

MurA product structure, Exposed region of phosphoenolpyruvate entry (PEP in red/tan on right)

CHAPTER IV

CONCLUSION AND FUTURE DIRECTIONS

The triazinoindol-benzimidazolone compounds show both high enzymatic potency and modestly low *M. tuberculosis* MIC's. The most kinetically soluble, 6665037, displays a high plasma protein binding, however, an animal model is needed to determine if serum levels reach a high enough concentration to prove effective against an infection. The lack of observed toxicity up to 100 μM in human dermal fibroblasts suggests a preliminary safety of the compounds.

Depending on the results of an animal model for serum concentration, modifications to the triazinoindol group would be in order. The original R2 substitutions only tested hydrophobic groups. With the crystal structures in hand, it is apparent than even a simple hydroxyl at R2 would both improve solubility and be able to hydrogen bond with Arg59. As the entire series is currently very hydrophobic, having the ClogP more in line with current drugs would likely increase their value as potential drugs. 6665037 has a ClogP of 4.12, which does conform to Lipinski's rules but is on the upper range of a histogram

of ClogP values of current drugs. The bulk of which range from 0.5 to 4.0. Adding a hydroxyl at R2 would lower the ClogP to 3.84, putting the compounds closer in line to the average.

Regardless of enzymatic or whole cell potency, a serum concentration animal model must be conducted to ensure either the current compounds or post-modification reach a threshold capable of killing *M. tuberculosis*. This will likely be an iterative process, of determining the murine serum levels, modifications if they are not sufficient, retesting enzymatic and whole cell potency, retesting cytotoxicity, and retesting in an animal model. It would not be unexpected if the final molecule looked markedly different than the starting scaffold.

The issue of patentability is also one to consider. As this compound series has been published and not patented, by virtue of the public announcement combined with a designated usage, it is unlikely the triazinoindol-benzimidazoles would be patentable as an antibiotic. While patent law is outside the scope of this body of work, a significant modification or outright replacement of the triazinoindol group could possibly allow for patentability

and a compound worth being investigated as a potential *M. tuberculosis* antibiotic.

Covalent modification of the active site cysteine of MurA has long been the direction of research relating to antibiotic development utilizing MurA as the enzyme target. This is understandable, given the success of fosfomycin. However, after decades of research there is not a single commercial analog of fosfomycin, or any other FDA approved covalent modifier. This is in contract to other classes of antibiotics. Beta-lactams contain well in excess of 50 examples that, while many are rarely or not used at all today, have been used to treat infections. The macrolides contain over 20 examples.

This is not to suggest that it is not feasible to develop a new commercial covalent modifier. However, with the absolute requirement for the presence of the active site cysteine and the lack of toxicity even at gram-sized doses of fosfomycin, fosfomycin either works well or doesn’t work at all. A simple, and not uncommon, cysteine mutation protects against fosfomycin with a minimal fitness cost. Enzymes, such as FosA, capable of deactivating fosfomycin can be overcome simply by increasing the dose. It can be argued that there is no

pressing need for a fosfomycin “upgrade”. There have certainly been multitudinous examples of covalent modifiers discovered and analyzed.

Because of this, a non-covalent inhibitor against MurA would be ideal to supplement fosfomycin. As has been laid out, MurA has very high sequence conservation against taxonomically broad species. A non-covalent inhibitor would likely have some degree of activity across pathogenic and non-pathogenic species. Not relying on the active site cysteine would make a mutational adaptation less damaging to the drug’s efficacy.

There have been a small number of non-covalent inhibitors published, however, none of them are potent enough to be considered, as they currently are, to be worth further evaluation[108]. Medicinal chemistry would need to be performed to modify the compounds to first improve their enzymatic inhibition.

As MurA has been heavily researched and many libraries screened, it may be a more viable option to evaluate non-covalent inhibitors published and use them as a starting point for modification. That said, screening has recently resulted in a new inhibitor scaffold from Eniyan[109]. In addition, D-cycloserine was found to

inhibit MurA and a D-cycloserine mimic forms the core of these new molecules. While the mode of inhibition has not yet been published, if these prove to be non-covalent modifiers they could steer MurA drug research into a new direction. One of the compounds is enzymatically potent enough to warrant further investigation as to its whole cell potency. If it does not rely on an active site cysteine, it may also prove efficacious against *M. tuberculosis*, whose wild-type contains an aspartate rather than a cysteine and is naturally resistant to fosfomycin.

REFERENCES

1. Sivendran S, Jones V, Sun D, Wang Y, Grzegorzewicz AE, Scherman MS, et al. Identification of triazinoindol-benzimidazolones as nanomolar inhibitors of the Mycobacterium tuberculosis enzyme TDP-6-deoxy-d-xylo-4-hexopyranosid-4-ulose 3,5-epimerase (RmlC). Bioorg Med Chem. 2010;18(2):896-908. Epub 2009/12/09. doi: 10.1016/j.bmc.2009.11.033. PubMed PMID: 19969466; PubMed Central PMCID: PMCPMC2818544.

2. Wang Y, Hess TN, Jones V, Zhou JZ, McNeil MR, Andrew McCammon J. Novel inhibitors of Mycobacterium tuberculosis dTDP-6-deoxy-L-lyxo-4-hexulose reductase (RmlD) identified by virtual screening. Bioorg Med Chem Lett. 2011;21(23):7064-7. Epub 2011/10/22. doi: 10.1016/j.bmcl.2011.09.094. PubMed PMID: 22014548; PubMed Central PMCID: PMCPMC3223023.

3. Bae J, Kim SM, Lee SB. Identification and characterization of 2-keto-3-deoxy-L-rhamnonate dehydrogenase belonging to the MDR superfamily from the thermoacidophilic bacterium Sulfobacillus thermosulfidooxidans: implications to L-rhamnose metabolism in archaea. Extremophiles. 2015;19(2):469-78.

Epub 2015/01/27. doi: 10.1007/s00792-015-0731-8. PubMed PMID: 25617114.

4. Usadel B, Kuschinsky AM, Rosso MG, Eckermann N, Pauly M. RHM2 is involved in mucilage pectin synthesis and is required for the development of the seed coat in Arabidopsis. Plant Physiol. 2004;134(1):286-95. Epub 2003/12/13. doi: 10.1104/pp.103.034314. PubMed PMID: 14671019; PubMed Central PMCID: PMCPMC316308.

5. Feng L, Shou Q, Butcher RA. Identification of a dTDP-rhamnose biosynthetic pathway that oscillates with the molting cycle in Caenorhabditis elegans. Biochem J. 2016;473(11):1507-21. Epub 2016/03/25. doi: 10.1042/BCJ20160142. PubMed PMID: 27009306; PubMed Central PMCID: PMCPMC4888466.

6. Parakkottil Chothi M, Duncan GA, Armirotti A, Abergel C, Gurnon JR, Van Etten JL, et al. Identification of an L-rhamnose synthetic pathway in two nucleocytoplasmic large DNA viruses. J Virol. 2010;84(17):8829-38. Epub 2010/06/12. doi: 10.1128/JVI.00770-10. PubMed PMID: 20538863; PubMed Central PMCID: PMCPMC2918987.

7. Giraud MF, Naismith JH. The rhamnose pathway. Curr Opin Struc Biol. 2000;10(6):687-96. doi: Doi

10.1016/S0959-440x(00)00145-7. PubMed PMID: WOS:000166509100010.

8. Maki M, Renkonen R. Biosynthesis of 6-deoxyhexose glycans in bacteria. Glycobiology. 2004;14(3):1R-15R. Epub 2003/12/25. doi: 10.1093/glycob/cwh040. PubMed PMID: 14693916.

9. Kim SM, Paek KH, Lee SB. Characterization of NADP+-specific L-rhamnose dehydrogenase from the thermoacidophilic Archaeon Thermoplasma acidophilum. Extremophiles. 2012;16(3):447-54. Epub 2012/04/07. doi: 10.1007/s00792-012-0444-1. PubMed PMID: 22481639.

10. Saffer AM, Carpita NC, Irish VF. Rhamnose-Containing Cell Wall Polymers Suppress Helical Plant Growth Independently of Microtubule Orientation. Curr Biol. 2017;27(15):2248-+. doi: 10.1016/j.cub.2017.06.032. PubMed PMID: WOS:000407034300021.

11. Rocchetta HL, Burrows LL, Lam JS. Genetics of O-antigen biosynthesis in Pseudomonas aeruginosa. Microbiol Mol Biol Rev. 1999;63(3):523-53. Epub 1999/09/08. PubMed PMID: 10477307; PubMed Central PMCID: PMCPMC103745.

12. Krause RM, Mc CM. Variation in the group-specific carbohydrate of group C hemolytic Streptococci. J Exp Med.

1962;116:131-40. Epub 1962/08/01. PubMed PMID: 14459434; PubMed Central PMCID: PMCPMC2137385.

13. Ma Y, Pan F, McNeil M. Formation of dTDP-rhamnose is essential for growth of mycobacteria. J Bacteriol. 2002;184(12):3392-5. Epub 2002/05/25. PubMed PMID: 12029057; PubMed Central PMCID: PMCPMC135104.

14. Hsu YH, Tagami T, Matsunaga K, Okuyama M, Suzuki T, Noda N, et al. Functional characterization of UDP-rhamnose-dependent rhamnosyltransferase involved in anthocyanin modification, a key enzyme determining blue coloration in Lobelia erinus. Plant J. 2017;89(2):325-37. doi: 10.1111/tpj.13387. PubMed PMID: WOS:000395810600011.

15. Oka T, Nemoto T, Jigami Y. Functional analysis of Arabidopsis thaliana RHM2/MUM4, a multidomain protein involved in UDP-D-glucose to UDP-L-rhamnose conversion. Journal of Biological Chemistry. 2007;282(8):5389-403. doi: 10.1074/jbc.M610196200. PubMed PMID: WOS:000244482300034.

16. Tonetti M, Zanardi D, Gurnon JR, Fruscione F, Armirotti A, Damonte G, et al. Paramecium bursaria Chlorella virus 1 encodes two enzymes involved in the biosynthesis of GDP-L-fucose and GDP-D-rhamnose. J Biol

Chem. 2003;278(24):21559-65. Epub 2003/04/08. doi: 10.1074/jbc.M301543200. PubMed PMID: 12679342.

17. Martinez V, Ingwers M, Smith J, Glushka J, Yang T, Bar-Peled M. Biosynthesis of UDP-4-keto-6-deoxyglucose and UDP-rhamnose in pathogenic fungi Magnaporthe grisea and Botryotinia fuckeliana. J Biol Chem. 2012;287(2):879-92. Epub 2011/11/22. doi: 10.1074/jbc.M111.287367. PubMed PMID: 22102281; PubMed Central PMCID: PMCPMC3256918.

18. Gulati M, Nobile CJ. Candida albicans biofilms: development, regulation, and molecular mechanisms. Microbes Infect. 2016;18(5):310-21. Epub 2016/01/26. doi: 10.1016/j.micinf.2016.01.002. PubMed PMID: 26806384; PubMed Central PMCID: PMCPMC4860025.

19. Madduri K, Waldron C, Merlo DJ. Rhamnose biosynthesis pathway supplies precursors for primary and secondary metabolism in Saccharopolyspora spinosa. J Bacteriol. 2001;183(19):5632-8. Epub 2001/09/07. doi: 10.1128/JB.183.19.5632-5638.2001. PubMed PMID: 11544225; PubMed Central PMCID: PMCPMC95454.

20. Zuccotti S, Zanardi D, Rosano C, Sturla L, Tonetti M, Bolognesi M. Kinetic and crystallographic analyses support a sequential-ordered bi bi catalytic mechanism for Escherichia coli glucose-1-phosphate

thymidylyltransferase. J Mol Biol. 2001;313(4):831-43. Epub 2001/11/08. doi: 10.1006/jmbi.2001.5073. PubMed PMID: 11697907.

21. Aguirre-Ramirez M, Medina G, Gonzalez-Valdez A, Grosso-Becerra V, Soberon-Chavez G. The Pseudomonas aeruginosa rmlBDAC operon, encoding dTDP-L-rhamnose biosynthetic enzymes, is regulated by the quorum-sensing transcriptional regulator RhlR and the alternative sigma factor sigmaS. Microbiology. 2012;158(Pt 4):908-16. Epub 2012/01/21. doi: 10.1099/mic.0.054726-0. PubMed PMID: 22262098.

22. Alderwick LJ, Harrison J, Lloyd GS, Birch HL. The Mycobacterial Cell Wall--Peptidoglycan and Arabinogalactan. Cold Spring Harb Perspect Med. 2015;5(8):a021113. Epub 2015/03/31. doi: 10.1101/cshperspect.a021113. PubMed PMID: 25818664; PubMed Central PMCID: PMCPMC4526729.

23. Brennan PJ. Structure, function, and biogenesis of the cell wall of Mycobacterium tuberculosis. Tuberculosis (Edinb). 2003;83(1-3):91-7. Epub 2003/05/22. PubMed PMID: 12758196.

24. Russell DG. Who puts the tubercle in tuberculosis? Nat Rev Microbiol. 2007;5(1):39-47. Epub 2006/12/13. doi: 10.1038/nrmicro1538. PubMed PMID: 17160001.

25. Roscigno G. Giorgio Roscigno--senior advisor to the Global Alliance for TB Drug Development. Interviewed by Pam Das. Lancet Infect Dis. 2002;2(6):377-80. Epub 2002/07/30. PubMed PMID: 12144902.

26. Goude R, Parish T. The genetics of cell wall biosynthesis in Mycobacterium tuberculosis. Future Microbiol. 2008;3(3):299-313. Epub 2008/05/29. doi: 10.2217/17460913.3.3.299. PubMed PMID: 18505396.

27. Norton BL, Holland DP. Current management options for latent tuberculosis: a review. Infect Drug Resist. 2012;5:163-73. Epub 2012/12/12. doi: 10.2147/IDR.S29180. PubMed PMID: 23226700; PubMed Central PMCID: PMCPMC3514970.

28. Grzegorzewicz AE, de Sousa-d'Auria C, McNeil MR, Huc-Claustre E, Jones V, Petit C, et al. Assembling of the Mycobacterium tuberculosis Cell Wall Core. J Biol Chem. 2016;291(36):18867-79. Epub 2016/07/16. doi: 10.1074/jbc.M116.739227. PubMed PMID: 27417139; PubMed Central PMCID: PMCPMC5009262.

29. Crick DC, Mahapatra S, Brennan PJ. Biosynthesis of the arabinogalactan-peptidoglycan complex of Mycobacterium tuberculosis. Glycobiology. 2001;11(9):107r-18r. doi: DOI 10.1093/glycob/11.9.107R. PubMed PMID: WOS:000171271800002.

30. Blankenfeldt W, Asuncion M, Lam JS, Naismith JH. The structural basis of the catalytic mechanism and regulation of glucose-1-phosphate thymidylyltransferase (RmlA). EMBO J. 2000;19(24):6652-63. Epub 2000/12/16. doi: 10.1093/emboj/19.24.6652. PubMed PMID: 11118200; PubMed Central PMCID: PMCPMC305900.

31. Allard ST, Beis K, Giraud MF, Hegeman AD, Gross JW, Wilmouth RC, et al. Toward a structural understanding of the dehydratase mechanism. Structure. 2002;10(1):81-92. Epub 2002/02/14. PubMed PMID: 11796113.

32. Allard ST, Giraud MF, Whitfield C, Graninger M, Messner P, Naismith JH. The crystal structure of dTDP-D-Glucose 4,6-dehydratase (RmlB) from Salmonella enterica serovar Typhimurium, the second enzyme in the dTDP-l-rhamnose pathway. J Mol Biol. 2001;307(1):283-95. Epub 2001/03/13. doi: 10.1006/jmbi.2000.4470. PubMed PMID: 11243820.

33. Allard ST, Giraud MF, Whitfield C, Messner P, Naismith JH. The purification, crystallization and structural elucidation of dTDP-D-glucose 4,6-dehydratase (RmlB), the second enzyme of the dTDP-L-rhamnose synthesis pathway from Salmonella enterica serovar typhimurium. Acta Crystallogr D Biol Crystallogr. 2000;56(Pt 2):222-5. Epub 2000/02/10. PubMed PMID: 10666612.

34. Giraud MF, Leonard GA, Field RA, Berlind C, Naismith JH. RmlC, the third enzyme of dTDP-L-rhamnose pathway, is a new class of epimerase. Nat Struct Biol. 2000;7(5):398-402. PubMed PMID: WOS:000086908800016.

35. Dong C, Major LL, Srikannathasan V, Errey JC, Giraud MF, Lam JS, et al. RmlC, a C3' and C5' carbohydrate epimerase, appears to operate via an intermediate with an unusual twist boat conformation. J Mol Biol. 2007;365(1):146-59. Epub 2006/10/19. doi: 10.1016/j.jmb.2006.09.063. PubMed PMID: 17046787; PubMed Central PMCID: PMCPMC1805628.

36. Qu H, Xin Y, Dong X, Ma Y. An rmlA gene encoding d-glucose-1-phosphate thymidylyltransferase is essential for mycobacterial growth. FEMS Microbiol Lett. 2007;275(2):237-43. Epub 2007/09/06. doi: 10.1111/j.1574-6968.2007.00890.x. PubMed PMID: 17784859.

37. Mills JA, Motichka K, Jucker M, Wu HP, Uhlik BC, Stern RJ, et al. Inactivation of the mycobacterial rhamnosyltransferase, which is needed for the formation of the arabinogalactan-peptidoglycan linker, leads to irreversible loss of viability. J Biol Chem. 2004;279(42):43540-6. Epub 2004/08/06. doi: 10.1074/jbc.M407782200. PubMed PMID: 15294902.

38. Bernal C, Palacin C, Boronat A, Imperial S. A colorimetric assay for the determination of 4-diphosphocytidyl-2-C-methyl-D-erythritol 4-phosphate synthase activity. Anal Biochem. 2005;337(1):55-61. Epub 2005/01/15. doi: 10.1016/j.ab.2004.10.011. PubMed PMID: 15649375.

39. Ma Y, Stern RJ, Scherman MS, Vissa VD, Yan W, Jones VC, et al. Drug targeting Mycobacterium tuberculosis cell wall synthesis: genetics of dTDP-rhamnose synthetic enzymes and development of a microtiter plate-based screen for inhibitors of conversion of dTDP-glucose to dTDP-rhamnose. Antimicrob Agents Chemother. 2001;45(5):1407-16. Epub 2001/04/17. doi: 10.1128/AAC.45.5.1407-1416.2001. PubMed PMID: 11302803; PubMed Central PMCID: PMCPMC90481.

40. Alphey MS, Pirrie L, Torrie LS, Boulkeroua WA, Gardiner M, Sarkar A, et al. Allosteric Competitive

Inhibitors of the Glucose-1-phosphate Thymidylyltransferase (RmlA) from Pseudomonas aeruginosa. Acs Chem Biol. 2013;8(2):387-96. doi: 10.1021/cb300426u. PubMed PMID: WOS:000315253700015.

41. Blankenfeldt W, Giraud MF, Leonard G, Rahim R, Creuzenet C, Lam JS, et al. The purification, crystallization and preliminary structural characterization of glucose-1-phosphate thymidylyltransferase (Rm1A), the first enzyme of the dTDP-L-rhamnose synthesis pathway from Pseudomonas aeruginosa. Acta Crystallogr D. 2000;56:1501-4. doi: Doi 10.1107/S0907444900010040. PubMed PMID: WOS:000165336100035.

42. Baumgartner J, Lee J, Halavaty AS, Minasov G, Anderson WF, Kuhn ML. Structure of the Bacillus anthracis dTDP-L-rhamnose-biosynthetic enzyme glucose-1-phosphate thymidylyltransferase (RfbA). Acta Crystallogr F Struct Biol Commun. 2017;73(Pt 11):621-8. Epub 2017/11/03. doi: 10.1107/S2053230X17015357. PubMed PMID: 29095156; PubMed Central PMCID: PMCPMC5683032.

43. van der Beek SL, Le Breton Y, Ferenbach AT, Chapman RN, van Aalten DM, Navratilova I, et al. GacA is essential for Group A Streptococcus and defines a new class of

monomeric dTDP-4-dehydrorhamnose reductases (RmlD). Mol Microbiol. 2015;98(5):946-62. Epub 2015/08/19. doi: 10.1111/mmi.13169. PubMed PMID: 26278404; PubMed Central PMCID: PMCPMC4832382.

44. Beis K, Allard ST, Hegeman AD, Murshudov G, Philp D, Naismith JH. The structure of NADH in the enzyme dTDP-d-glucose dehydratase (RmlB). J Am Chem Soc. 2003;125(39):11872-8. Epub 2003/09/25. doi: 10.1021/ja035796r. PubMed PMID: 14505409.

45. Blankenfeldt W, Kerr ID, Giraud MF, McMiken HJ, Leonard G, Whitfield C, et al. Variation on a theme of SDR. dTDP-6-deoxy-L- lyxo-4-hexulose reductase (RmlD) shows a new Mg2+-dependent dimerization mode. Structure. 2002;10(6):773-86. Epub 2002/06/12. PubMed PMID: 12057193.

46. Anderson AC. The process of structure-based drug design. Chem Biol. 2003;10(9):787-97. Epub 2003/10/03. PubMed PMID: 14522049.

47. Oprea TI. Current trends in lead discovery: are we looking for the appropriate properties? Mol Divers. 2002;5(4):199-208. Epub 2003/01/29. PubMed PMID: 12549672.

48. Elander RP. Industrial production of beta-lactam antibiotics. Appl Microbiol Biotechnol. 2003;61(5-6):385-

92. Epub 2003/04/08. doi: 10.1007/s00253-003-1274-y. PubMed PMID: 12679848.

49. Fleming A. On the antibacterial action of cultures of a penicillium, with special reference to their use in the isolation of B. influenzae. 1929. Bull World Health Organ. 2001;79(8):780-90. Epub 2001/09/08. PubMed PMID: 11545337; PubMed Central PMCID: PMCPMC2566493.

50. Diggins FW. The true history of the discovery of penicillin, with refutation of the misinformation in the literature. Br J Biomed Sci. 1999;56(2):83-93. Epub 2000/03/01. PubMed PMID: 10695047.

51. Blumberg PM, Strominger JL. Interaction of penicillin with the bacterial cell: penicillin-binding proteins and penicillin-sensitive enzymes. Bacteriol Rev. 1974;38(3):291-335. Epub 1974/09/01. PubMed PMID: 4608953; PubMed Central PMCID: PMCPMC413858.

52. Spratt BG, Strominger JL. Identification of the major penicillin-binding proteins of Escherichia coli as D-alanine carboxypeptidase IA. J Bacteriol. 1976;127(1):660-3. Epub 1976/07/01. PubMed PMID: 776946; PubMed Central PMCID: PMCPMC233099.

53. Tomasz A. The mechanism of the irreversible antimicrobial effects of penicillins: how the beta-lactam

antibiotics kill and lyse bacteria. Annu Rev Microbiol. 1979;33:113-37. Epub 1979/01/01. doi: 10.1146/annurev.mi.33.100179.000553. PubMed PMID: 40528.

54. Reading C, Cole M. Clavulanic acid: a beta-lactamase-inhiting beta-lactam from Streptomyces clavuligerus. Antimicrob Agents Chemother. 1977;11(5):852-7. Epub 1977/05/01. PubMed PMID: 879738; PubMed Central PMCID: PMCPMC352086.

55. Wang F, Cassidy C, Sacchettini JC. Crystal structure and activity studies of the Mycobacterium tuberculosis beta-lactamase reveal its critical role in resistance to beta-lactam antibiotics. Antimicrob Agents Chemother. 2006;50(8):2762-71. Epub 2006/07/28. doi: 10.1128/AAC.00320-06. PubMed PMID: 16870770; PubMed Central PMCID: PMCPMC1538687.

56. Bhagirath AY, Li Y, Somayajula D, Dadashi M, Badr S, Duan K. Cystic fibrosis lung environment and Pseudomonas aeruginosa infection. BMC Pulm Med. 2016;16(1):174. Epub 2016/12/07. doi: 10.1186/s12890-016-0339-5. PubMed PMID: 27919253; PubMed Central PMCID: PMCPMC5139081.

57. Brown ED, Vivas EI, Walsh CT, Kolter R. Mura (Murz), the Enzyme That Catalyzes the First Committed Step in Peptidoglycan Biosynthesis, Is Essential in Escherichia-

Coli. Journal of Bacteriology. 1995;177(14):4194-7. doi: DOI 10.1128/jb.177.14.4194-4197.1995. PubMed PMID: WOS:A1995RH81000048.

58. Dube S, Nanda K, Rani R, Kaur NJ, Nagpal JK, Upadhyay DJ, et al. UDP-N-acetylglucosamine enolpyruvyl transferase from Pseudomonas aeruginosa. World J Microb Biot. 2010;26(9):1623-9. doi: 10.1007/s11274-010-0338-2. PubMed PMID: WOS:000280642800010.

59. Eschenburg S, Priestman MA, Abdul-Latif FA, Delachaume C, Fassy F, Schonbrunn E. A novel inhibitor that suspends the induced fit mechanism of UDP-N-acetylglucosamine enolpyruvyl transferase (MurA). J Biol Chem. 2005;280(14):14070-5. Epub 2005/02/11. doi: 10.1074/jbc.M414412200. PubMed PMID: 15701635.

60. Webb MR. A continuous spectrophotometric assay for inorganic phosphate and for measuring phosphate release kinetics in biological systems. Proc Natl Acad Sci U S A. 1992;89(11):4884-7. Epub 1992/06/01. PubMed PMID: 1534409; PubMed Central PMCID: PMCPMC49192.

61. van Heijenoort J. Lipid intermediates in the biosynthesis of bacterial peptidoglycan. Microbiol Mol Biol Rev. 2007;71(4):620-35. Epub 2007/12/08. doi:

10.1128/MMBR.00016-07. PubMed PMID: 18063720; PubMed Central PMCID: PMCPMC2168651.

62. Typas A, Banzhaf M, Gross CA, Vollmer W. From the regulation of peptidoglycan synthesis to bacterial growth and morphology. Nat Rev Microbiol. 2011;10(2):123-36. Epub 2011/12/29. doi: 10.1038/nrmicro2677. PubMed PMID: 22203377; PubMed Central PMCID: PMCPMC5433867.

63. Typas A, Banzhaf M, van den Berg van Saparoea B, Verheul J, Biboy J, Nichols RJ, et al. Regulation of peptidoglycan synthesis by outer-membrane proteins. Cell. 2010;143(7):1097-109. Epub 2010/12/25. doi: 10.1016/j.cell.2010.11.038. PubMed PMID: 21183073; PubMed Central PMCID: PMCPMC3060616.

64. Trapnell BC, McColley SA, Kissner DG, Rolfe MW, Rosen JM, McKevitt M, et al. Fosfomycin/tobramycin for inhalation in patients with cystic fibrosis with pseudomonas airway infection. Am J Respir Crit Care Med. 2012;185(2):171-8. Epub 2011/11/19. doi: 10.1164/rccm.201105-0924OC. PubMed PMID: 22095545; PubMed Central PMCID: PMCPMC3361752.

65. Han H, Yang Y, Olesen SH, Becker A, Betzi S, Schonbrunn E. The fungal product terreic acid is a covalent inhibitor of the bacterial cell wall biosynthetic

enzyme UDP-N-acetylglucosamine 1-carboxyvinyltransferase (MurA). Biochemistry. 2010;49(19):4276-82. Epub 2010/04/16. doi: 10.1021/bi100365b. PubMed PMID: 20392080; PubMed Central PMCID: PMCPMC2884014.

66. Olesen SH, Ingles DJ, Yang Y, Schonbrunn E. Differential antibacterial properties of the MurA inhibitors terreic acid and fosfomycin. J Basic Microbiol. 2014;54(4):322-6. Epub 2013/05/21. doi: 10.1002/jobm.201200617. PubMed PMID: 23686727; PubMed Central PMCID: PMCPMC4610358.

67. Shigetomi K, Olesen SH, Yang Y, Mitsuhashi S, Schonbrunn E, Ubukata M. MurA as a Primary Target of Tulipalin B and 6-Tuliposide B. Biosci Biotech Bioch. 2013;77(12):2517-9. doi: 10.1271/bbb.130663. PubMed PMID: WOS:000330086500033.

68. Shigetomi K, Kishimoto T, Shoji K, Ubukata M. First total synthesis of 6-tuliposide B. Tetrahedron-Asymmetr. 2008;19(12):1444-9. doi: 10.1016/j.tetasy.2008.05.019. PubMed PMID: WOS:000258046200009.

69. Shigetomi K, Kishimoto T, Shoji K, Ubukata M. Synthesis of tulipalin B and 1-O-methyl-6-tuliposide B. Heterocycles. 2006;69(1):63-+. PubMed PMID: WOS:000243651000005.

70. Shigetomi K, Shoji K, Mitsuhashi S, Ubukata M. The antibacterial properties of 6-tuliposide B. Synthesis of 6-tuliposide B analogues and structure-activity relationship. Phytochemistry. 2010;71(2-3):312-24. Epub 2009/11/27. doi: 10.1016/j.phytochem.2009.10.008. PubMed PMID: 19939419.

71. Steinbach A, Scheidig AJ, Klein CD. The unusual binding mode of cnicin to the antibacterial target enzyme MurA revealed by X-ray crystallography. J Med Chem. 2008;51(16):5143-7. Epub 2008/08/05. doi: 10.1021/jm800609p. PubMed PMID: 18672863.

72. Bach SM, Fortuna MA, Attarian R, de Trimarco JT, Catalan CA, Av-Gay Y, et al. Antibacterial and cytotoxic activities of the sesquiterpene lactones cnicin and onopordopicrin. Nat Prod Commun. 2011;6(2):163-6. Epub 2011/03/24. PubMed PMID: 21425665.

73. Kieser KJ, Baranowski C, Chao MC, Long JE, Sassetti CM, Waldor MK, et al. Peptidoglycan synthesis in Mycobacterium tuberculosis is organized into networks with varying drug susceptibility. Proc Natl Acad Sci U S A. 2015;112(42):13087-92. Epub 2015/10/07. doi: 10.1073/pnas.1514135112. PubMed PMID: 26438867; PubMed Central PMCID: PMCPMC4620856.

74. Abrahams KA, Besra GS. Mycobacterial cell wall biosynthesis: a multifaceted antibiotic target. Parasitology. 2018;145(2):116-33. Epub 2016/12/16. doi: 10.1017/S0031182016002377. PubMed PMID: 27976597; PubMed Central PMCID: PMCPMC5964476.

75. Li W, Xin Y, McNeil MR, Ma Y. rmlB and rmlC genes are essential for growth of mycobacteria. Biochem Biophys Res Commun. 2006;342(1):170-8. Epub 2006/02/14. doi: 10.1016/j.bbrc.2006.01.130. PubMed PMID: 16472764.

76. Kantardjieff KA, Kim CY, Naranjo C, Waldo GS, Lekin T, Segelke BW, et al. Mycobacterium tuberculosis RmlC epimerase (Rv3465): a promising drug-target structure in the rhamnose pathway. Acta Crystallogr D Biol Crystallogr. 2004;60(Pt 5):895-902. Epub 2004/04/23. doi: 10.1107/S0907444904005323. PubMed PMID: 15103135.

77. Otwinowski Z, Minor W. Processing of X-ray diffraction data collected in oscillation mode. Method Enzymol. 1997;276:307-26. doi: Doi 10.1016/S0076-6879(97)76066-X. PubMed PMID: WOS:A1997BH42P00020.

78. Adams PD, Grosse-Kunstleve RW, Hung LW, Ioerger TR, McCoy AJ, Moriarty NW, et al. PHENIX: building new software for automated crystallographic structure determination. Acta Crystallogr D Biol Crystallogr.

2002;58(Pt 11):1948-54. Epub 2002/10/24. PubMed PMID: 12393927.

79. Emsley P, Cowtan K. Coot: model-building tools for molecular graphics. Acta Crystallogr D Biol Crystallogr. 2004;60(Pt 12 Pt 1):2126-32. Epub 2004/12/02. doi: 10.1107/S0907444904019158. PubMed PMID: 15572765.

80. Pettersen EF, Goddard TD, Huang CC, Couch GS, Greenblatt DM, Meng EC, et al. UCSF Chimera--a visualization system for exploratory research and analysis. J Comput Chem. 2004;25(13):1605-12. Epub 2004/07/21. doi: 10.1002/jcc.20084. PubMed PMID: 15264254.

81. Diehl KH, Hull R, Morton D, Pfister R, Rabemampianina Y, Smith D, et al. A good practice guide to the administration of substances and removal of blood, including routes and volumes. J Appl Toxicol. 2001;21(1):15-23. Epub 2001/02/17. PubMed PMID: 11180276.

82. Zhang Y, Huo M, Zhou J, Xie S. PKSolver: An add-in program for pharmacokinetic and pharmacodynamic data analysis in Microsoft Excel. Comput Methods Programs Biomed. 2010;99(3):306-14. Epub 2010/02/24. doi: 10.1016/j.cmpb.2010.01.007. PubMed PMID: 20176408.

83. Chandler D. Interfaces and the driving force of hydrophobic assembly. Nature. 2005;437(7059):640-7. Epub

2005/09/30. doi: 10.1038/nature04162. PubMed PMID: 16193038.

84. Schufle JA. Water - a Comprehensive Treatise, Vol 7, Water and Aqueous-Solutions at Subzero Temperatures - Franks,F. Journal of the American Chemical Society. 1983;105(21):6532-. PubMed PMID: WOS:A1983RN40600055.

85. Kauzmann W. Some Factors in the Interpretation of Protein Denaturation. Adv Protein Chem. 1959;14:1-63. doi: Doi 10.1016/S0065-3233(08)60608-7. PubMed PMID: WOS:A1959WF06400001.

86. Tanford C. The hydrophobic effect and the organization of living matter. Science. 1978;200(4345):1012-8. Epub 1978/06/02. PubMed PMID: 653353.

87. Nemethy G, Steinberg IZ, Scheraga HA. Influence of Water Structure and of Hydrophobic Interactions on the Strength of Side-Chain Hydrogen Bonds in Proteins. Biopolymers. 1963;1(1):43-69. doi: DOI 10.1002/bip.360010107. PubMed PMID: WOS:A1963WS27900005.

88. Bennaim A, Wilf J, Yaacobi M. Hydrophobic Interaction in Light and Heavy-Water. J Phys Chem-Us. 1973;77(1):95-102. doi: DOI 10.1021/j100620a021. PubMed PMID: WOS:A1973O412400021.

89. Marcelja S, Mitchell DJ, Ninham BW, Sculley MJ. Role of Solvent Structure in Solution Theory. J Chem Soc Farad T 2. 1977;73:630-48. doi: DOI 10.1039/f29777300630. PubMed PMID: WOS:A1977DG41000006.

90. Chan DYC, Mitchell DJ, Ninham BW, Pailthorpe BA. Short-Range Interactions Mediated by a Solvent with Surface Adhesion. Mol Phys. 1978;35(6):1669-79. doi: Doi 10.1080/00268977800101251. PubMed PMID: WOS:A1978FH31000013.

91. Rossky PJ, Friedman HL. Benzene-Benzene Interaction in Aqueous-Solution. J Phys Chem-Us. 1980;84(6):587-9. doi: DOI 10.1021/j100443a005. PubMed PMID: WOS:A1980JK57900005.

92. Israelachvili J, Pashley R. The Hydrophobic Interaction Is Long-Range, Decaying Exponentially with Distance. Nature. 1982;300(5890):341-2. doi: DOI 10.1038/300341a0. PubMed PMID: WOS:A1982PR77400037.

93. Savjani KT, Gajjar AK, Savjani JK. Drug solubility: importance and enhancement techniques. ISRN Pharm. 2012;2012:195727. Epub 2012/07/26. doi: 10.5402/2012/195727. PubMed PMID: 22830056; PubMed Central PMCID: PMCPMC3399483.

94. Holten KB, Onusko EM. Appropriate prescribing of oral beta-lactam antibiotics. Am Fam Physician. 2000;62(3):611-20. Epub 2000/08/19. PubMed PMID: 10950216.

95. Berrazeg M, Jeannot K, Ntsogo Enguene VY, Broutin I, Loeffert S, Fournier D, et al. Mutations in beta-Lactamase AmpC Increase Resistance of Pseudomonas aeruginosa Isolates to Antipseudomonal Cephalosporins. Antimicrob Agents Chemother. 2015;59(10):6248-55. Epub 2015/08/08. doi: 10.1128/AAC.00825-15. PubMed PMID: 26248364; PubMed Central PMCID: PMCPMC4576058.

96. Jovcic B, Lepsanovic Z, Suljagic V, Rackov G, Begovic J, Topisirovic L, et al. Emergence of NDM-1 Metallo-beta-Lactamase in Pseudomonas aeruginosa Clinical Isolates from Serbia. Antimicrob Agents Ch. 2011;55(8):3929-31. doi: 10.1128/Aac.00226-11. PubMed PMID: WOS:000292733800036.

97. Wroblewski AE, Bak-Sypien II. New analogues of fosfomycin-synthesis of diethyl (1R,2R)- and (1S,2R)-1,2-epoxy-3-hydroxypropylphosphonates. Tetrahedron-Asymmetr. 2007;18(4):520-6. doi: 10.1016/j.tetasy.2007.02.006. PubMed PMID: WOS:000245836500012.

98. Jacobson S, Noa LJ, Ahmed S, Wallace MR. Efficacy and Safety of Oral Fosfomycin for Urinary Tract Infections in Hospitalized Patients. Antimicrob Agents Ch.

2016;60(3):1952-. doi: 10.1128/Aac.02971-15. PubMed PMID: WOS:000376490800108.

99. Sardar A, Basireddy SR, Navaz A, Singh M, Kabra V. Comparative Evaluation of Fosfomycin Activity with other Antimicrobial Agents against E.coli Isolates from Urinary Tract Infections. J Clin Diagn Res. 2017;11(2):DC26-DC9. Epub 2017/04/08. doi: 10.7860/JCDR/2017/23644.9440. PubMed PMID: 28384863; PubMed Central PMCID: PMCPMC5376875.

100. Kim DH, Lees WJ, Kempsell KE, Lane WS, Duncan K, Walsh CT. Characterization of a Cys115 to Asp substitution in the Escherichia coli cell wall biosynthetic enzyme UDP-GlcNAc enolpyruvyl transferase (MurA) that confers resistance to inactivation by the antibiotic fosfomycin. Biochemistry. 1996;35(15):4923-8. doi: DOI 10.1021/bi952937w. PubMed PMID: WOS:A1996UF52100032.

101. De Smet KA, Kempsell KE, Gallagher A, Duncan K, Young DB. Alteration of a single amino acid residue reverses fosfomycin resistance of recombinant MurA from Mycobacterium tuberculosis. Microbiology. 1999;145 (Pt 11):3177-84. Epub 1999/12/10. doi: 10.1099/00221287-145-11-3177. PubMed PMID: 10589726.

102. Mizyed S, Oddone A, Byczynski B, Hughes DW, Berti PJ. UDP-N-acetylmuramic acid (UDP-MurNAc) is a potent

inhibitor of MurA (enolpyruvyl-UDP-GlcNAc synthase). Biochemistry. 2005;44(10):4011-7. doi: 10.1021/bi047704w. PubMed PMID: WOS:000227629300036.

103. Eschenburg S, Kabsch W, Healy ML, Schonbrunn E. A new view of the mechanisms of UDP-N-acetylglucosamine enolpyruvyl transferase (MurA) and 5-enolpyruvylshikimate-3-phosphate synthase (AroA) derived from X-ray structures of their tetrahedral reaction intermediate states. Journal of Biological Chemistry. 2003;278(49):49215-22. doi: 10.1074/jbc.M309741200. PubMed PMID: WOS:000186829000086.

104. Huth ME, Ricci AJ, Cheng AG. Mechanisms of aminoglycoside ototoxicity and targets of hair cell protection. Int J Otolaryngol. 2011;2011:937861. Epub 2011/11/29. doi: 10.1155/2011/937861. PubMed PMID: 22121370; PubMed Central PMCID: PMCPMC3202092.

105. Orlando R, Piccoli P, De Martin S, Padrini R, Palatini P. Effect of the CYP3A4 inhibitor erythromycin on the pharmacokinetics of lignocaine and its pharmacologically active metabolites in subjects with normal and impaired liver function. Br J Clin Pharmacol. 2003;55(1):86-93. Epub 2003/01/22. PubMed PMID: 12534644; PubMed Central PMCID: PMCPMC1884183.

106. Ress BD, Gross EM. Irreversible sensorineural hearing loss as a result of azithromycin ototoxicity - A case report. Ann Oto Rhinol Laryn. 2000;109(4):435-7. doi: Doi 10.1177/000348940010900416. PubMed PMID: WOS:000086418900016.

107. Hong S, Harris KA, Fanning KD, Sarachan KL, Frohlich KM, Agris PF. Evidence That Antibiotics Bind to Human Mitochondrial Ribosomal RNA Has Implications for Aminoglycoside Toxicity. Journal of Biological Chemistry. 2015;290(31):19273-86. doi: 10.1074/jbc.M115.655092. PubMed PMID: WOS:000358781100040.

108. Baum EZ, Montenegro DA, Licata L, Turchi I, Webb GC, Foleno BD, et al. Identification and characterization of new inhibitors of the Escherichia coli MurA enzyme. Antimicrob Agents Ch. 2001;45(11):3182-8. doi: Doi 10.1128/Aac.45.11.3182-3188.2001. PubMed PMID: WOS:000171664900031.

109. Eniyan K, Kumar A, Rayasam GV, Perdih A, Bajpai U. Development of a one-pot assay for screening and identification of Mur pathway inhibitors in Mycobacterium tuberculosis. Sci Rep. 2016;6:35134. Epub 2016/10/14. doi: 10.1038/srep35134. PubMed PMID: 27734910; PubMed Central PMCID: PMCPMC5062083.

APPENDIX

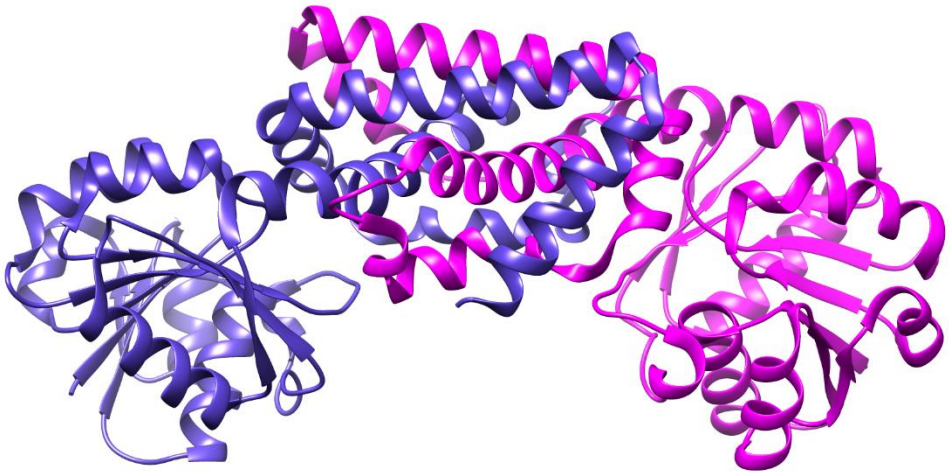

Structure of M. tubcerulosis prephenate dehydrogenase in the apo form